U–Pb age constraints on the Carboniferous-Permian transition in continental basins of eastern equatorial Pangaea (France): implications for the depositional history and correlations across the late Variscan Belt

Mathilde Mercuzot, Camille Rossignol, Sylvie Bourquin, Jahandar Ramezani, Céline Ducassou, Marc Poujol, Laurent Beccaletto, Pierre Pellenard

Accepted Manuscript

Journal of the Geological Society

U–Pb age constraints on the Carboniferous-Permian transition in continental basins of eastern equatorial Pangaea (France): implications for the depositional history and correlations across the late Variscan Belt

Mathilde Mercuzot, Camille Rossignol, Sylvie Bourquin, Jahandar Ramezani, Céline Ducassou, Marc Poujol, Laurent Beccaletto & Pierre Pellenard

DOI: https://doi.org/10.1144/jgs2023-075

To access the most recent version of this article, please click the DOI URL in the line above. When citing this article please include the above DOI.

Received 24 May 2023
Revised 5 August 2023
Accepted 20 August 2023

Supplementary material at https://doi.org/10.6084/m9.figshare.c.6805228

U–Pb age constraints on the Carboniferous-Permian transition in continental basins of eastern equatorial Pangaea (France): implications for the depositional history and correlations across the late Variscan Belt

Mathilde Mercuzot[1,2*], Camille Rossignol[3], Sylvie Bourquin[1], Jahandar Ramezani[4], Céline Ducassou[1], Marc Poujol[1], Laurent Beccaletto[5], Pierre Pellenard[6]

[1]*Univ Rennes, CNRS, Géosciences Rennes - UMR 6118, F-35000, Rennes, France*

[2]*EPOC/ Bordeaux-INP – UMR5805 EPOC, University of Bordeaux, Pessac, France*

[3]*Dipartimento di Scienze Chimiche e Geologiche, Università degli studi di Cagliari, Italy*

[4]*Department of Earth, Atmospheric and Planetary Sciences, Massachusetts Institute of Technology, Cambridge, Massachusetts 02139, USA*

[5]*BRGM, F-45060 Orléans, France*

[6]*Biogéosciences, UMR 6282, CNRS, Université de Bourgogne, 6 Bd Gabriel, F-21000 Dijon, France*

ORCID ID: MM: 0000-0002-7872-6771; CR: 0000-0003-0082-4854; SB: 0000-0002-2802-9548; JR: 0000-0002-5856-1471; CD: 0000-0002-3951-352X; MP: 0000-0001-8682-2926; LB: 0000-0003-2132-1738; PP: 0000-0002-1452-2569

**Corresponding author (e-mail: mathilde.mercuzot@outlook.com)*

Abbreviated title: U–Pb ages in European late Paleozoic basins

Abstract

Intramountain late Carboniferous–Permian basins of western Europe developed during the latest orogenic stages of the Variscan Mountain Belt in eastern Pangaea, at equatorial palaeolatitudes. Their stratigraphic framework is mainly based on continental subdivisions (e.g. Stephanian and Autunian continental stages), which can be contentious due to biostratigraphic biases, resulting in long-distance diachronous subdivisions. To provide precise inter-basinal and global correlations to the internationally recognized chronostratigraphic marine stages, this study reports new U–Pb geochronology from the Aumance and Decize–La Machine basins, located in the northern French Massif Central. Zircon grains

extracted from three volcanic ash-fall layers give weighted mean $^{206}Pb/^{238}U$ ages of 299.11 ± 0.35 Ma; 298.73 ± 0.36 Ma and 298.59 ± 0.35 Ma (2σ total propagated uncertainty) by the chemical abrasion–isotope dilution–thermal ionization mass spectrometry (CA-ID-TIMS) method, coinciding with the Carboniferous–Permian transition (Gzhelian and Asselian stages). These ages imply that the northern Massif Central basins developed synchronously in relatively short periods of time (<10 Myr), reflecting substantial sedimentation rates. Finally, the new chronology of infilling of these basins confirms that they were connected during the late Carboniferous and early Permian periods, improving the knowledge on the late-orogenic Variscan geodynamic setting in this area.

Supplementary material: U–Pb analytical results are available at

The late Carboniferous to early Permian sedimentary record is of major importance in documenting one of the most prominent climatic upheavals of the Phanerozoic Eon, i.e. the Late Paleozoic Ice Age (LPIA). The acme of this glaciation (ca. 298–295 Ma; e.g. Isbell *et al.* 2012; Soreghan *et al.* 2019) was followed by the transition from an icehouse to a greenhouse climate mode, culminating in hothouse conditions by the beginning of the Mesozoic (e.g. Chumakov and Zharkov 2002; Foster *et al.* 2017). The late Carboniferous to early Permian period also corresponded to major tectonic movements in Europe, marking the final stages of the Variscan Orogeny, and witnessed extensive explosive volcanism, especially in European basins (McCann 2008; Timmerman *et al.* 2009), that could have enhanced the glaciation (Soreghan *et al.* 2019). In eastern equatorial Pangaea and specifically in present-day Europe, numerous continental sedimentary basins (Fig. 1a) were initiated by the tectonic processes associated with the collapse of the Variscan Belt (e.g. Ménard and Molnar 1988; Wilson *et al.* 2004; Stampfli and Kozur 2006; Pellenard *et al.* 2017). Ongoing efforts to document the basin evolution, palaeogeography, depositional environments, and local to regional climate signals have been hampered by a lack of high-precision radioisotopic ages, preventing the construction of a robust chronostratigraphic framework, and hence precise regional and global correlations (e.g. Müller *et al.* 2006; Izart *et al.* 2012; Garel *et al.* 2017; Lützner *et al.* 2021; Mercuzot *et al.* 2021b). Many correlations across the late Carboniferous to Permian (C–P) European basins still rely on the use of regional stages based on continental biostratigraphy. These stages are mostly based on floral and faunal biozonations, such as macrofloras, pollens, spores and insects, which are environment-dependent, hence resulting in low temporal resolution, diachronism (e.g. Broutin *et al.* 1999) and contentious correlations. High-precision radioisotope geochronology has so far been available from a limited number of C–P basins of eastern Pangaea and some have produced ages differing to those previously inferred from biostratigraphic data, especially in the Permian Period (e.g. Opluštil *et al.* 2016a; Pellenard *et al.* 2017; Jirásek *et al.* 2018; Lützner *et al.* 2021). Consequently, accurate inter-basinal correlations across the Variscan continental realm and to the marine-based Standard Global Chronostratigraphic Scale will rely on systematic, high-precision geochronological efforts (e.g. Lucas and Shen 2018; Shen *et al.* 2019; Schneider *et al.* 2020).

Only then accurate constraints can be placed on the timing, drivers and dynamics of the contemporaneous LPIA climate and Variscan geodynamic events at the required resolution.

The structural and palaeoenvironmental settings of C–P basins of the northern Massif Central (France, Fig. 1b) have been re-evaluated and documented in a number of recent studies (Beccaletto *et al.* 2015; Ducassou *et al.* 2019; Garel *et al.* 2017; Mercuzot *et al.* 2021a, 2021b, 2022; Luccisano et al., 2022). Two of these basins, referred to as the Aumance and Decize–La Machine basins, exhibit significant thickness of late Carboniferous to Permian sedimentary successions (e.g. Marteau 1983; Donsimoni 1990). In the Decize–La Machine Basin, geochronological investigations using zircon and apatite U–Pb analyses by Laser Ablation–Inductively Coupled Plasma–Mass Spectrometry (LA–ICP–MS) have shown late Gzhelian to late Sakmarian depositional ages (i.e. 299 ± 2 Ma to 295 ± 5 Ma, Ducassou *et al.* 2019). These geochronological results have shown that C–P basins of the northern Massif Central are characterized by short time-span of deposition and high sediment accumulation rates (e.g. Pellenard *et al.* 2017; Ducassou *et al.* 2019), but a higher temporal resolution is still required for inter-basinal and regional correlations with other C–P basins of the Variscan Belt (Lützner *et al.* 2021).

In order to provide accurate depositional age constraints for the Aumance and Decize–La Machine siliciclastic sedimentary successions, this study presents new U–Pb geochronology by the high-precision Chemical Abrasion–Isotope Dilution–Thermal Ionization Mass Spectrometry (CA–ID–TIMS) method, used on zircon grains from interbedded volcanogenic deposits. The objectives are twofold: (i) refining the chronostratigraphy of a reference borehole in the Decize–La Machine Basin, the LY–F well, drilled in the Lucenay-lès-Aix Area (Fig. 2a, Ducassou *et al.* 2019), and (ii) providing the first high-precision age for the Aumance Basin (Fig. 2b). These results then allow direct correlation between the two basins, as well as with other well-dated C–P basins of the Variscan Belt, including the Autun Basin located in the direct vicinity (Fig. 1b), and to quantify sediment accumulation rates to better constraint the basin dynamics. The results serve as a keystone for further high-resolution studies documenting the late Paleozoic palaeoenvironmental, palaeoclimatic, and geodynamic evolution throughout Europe and beyond.

Geological setting

Late Carboniferous-Permian geodynamic and climate evolution in western Europe

The intramountain C–P basins of western Europe (Fig. 1a) formed during the syn- to post-tectonic stages of the Variscan Orogeny (Malavieille *et al.* 1990; Faure *et al.* 2009), during the late Gzhelian to middle Artinskian stages, from ca. 304 to 284 Ma (Schneider *et al.* 2006). This period corresponded to the culmination and subsequent demise of the penultimate global icehouse period, the LPIA (Fluteau *et al.* 2001; Chumakov and Zharkov 2002; Roscher and Schneider 2006; Fielding *et al.* 2008; Bishop *et al.* 2010; Isbell *et al.* 2012; Montañez and Poulsen 2013; Kent and Muttoni 2020). Most of the C–P basins exposed in the present-day Czech Republic, Poland, Germany, Switzerland, France, Italy, Spain and Portugal, developed along major Variscan faults (e.g. Schneider and Scholze 2018) at near-equatorial latitudes and exhibit strike-slip or hemi-graben geometries (e.g. Malavieille *et al.* 1990; Mascle 1990; Van Den Driessche and Brun 1992; Faure 1995; Stollhofen 1998; Lloret *et al.* 2018). Multiproxy studies of climate evolution in these low-latitude basins have mostly documented humid/arid cycles, punctuated by warmer episodes (e.g. Roscher and Schneider 2006; Schneider *et al.* 2006; Pochat and Van Den Driessche 2011; Izart *et al.* 2012; Cecil *et al.* 2014; Michel *et al.* 2015; Garel *et al.* 2017; Mujal *et al.* 2018; Trümper *et al.* 2020; Pfeifer *et al.* 2020, 2021; Mercuzot *et al.* 2021b).

The latest Carboniferous–early Permian collapse of the Variscan Belt was associated with a substantial intraplate magmatism between 305 and 290 Ma (Neumann *et al.* 2004), with a peak in volcanic activity around 290 Ma (Timmerman 2004; Timmerman *et al.* 2009), which tended to subside during the Permian Period, yet remaining substantial until the Triassic/Jurassic periods. This magmatic activity was due to the partial melting of the upper asthenosphere, likely resulting from the reorganization of the mantle convection (asthenosphere upwelling) because of a subducted slab detachment (Cloetingh *et al.* 2007). The mantle-derived magmatism was locally associated with substantial crustal assimilation (Bonin 1990; Bonin *et al.* 1993; Marx *et al.* 1995; Benek *et al.* 1996; Breitkreuz and Kennedy 1999; Neumann *et al.* 2004). The magmatic products have geochemical affinities characteristic of orogenic to anorogenic settings, with a broad compositional trend from mafic in northern Europe, to felsic in western and southern Europe (Timmerman 2004). Permian igneous rocks are predominantly alkaline in the

external zones of the belt (i.e. north of the Variscan Front, Fig. 1a), and calk-alkaline to alkaline in the inner zones (i.e. south of the Variscan Front; Spillmann and Büchi 1993; Bonin *et al.* 1998). Permian mafic plutons with a tholeiitic affinity have also been reported from a range of crustal levels (Vielzeuf and Pin 1989; Hermann 1997; Tribuzio *et al.* 1999, 2009; Monjoie *et al.* 2007).

In northern and eastern Europe, the Early Permian intrusive and extrusive magmatic activity was particularly pronounced in the basins located to the north of the Variscan Front (Variscan Foredeep and area of the future Northern and Southern Permian Basins; Copestake et al. 2003; Doornenbal and Stevenson 2010). Southwards of the Variscan Front, the European continental C–P basins related to major Variscan structures also witnessed numerous volcanic episodes intercalated in the Permian sedimentary successions, especially during in the lower Permian (Bixel 1988; Zheng *et al.* 1992; Cortesogno *et al.* 1998; Timmerman 2004; Pereira *et al.* 2014; Rodríguez-Méndez *et al.* 2014). The C–P magmatism also included explosive volcanism producing tuffs and tuffaceous deposits (e.g. Schneider and Scholze 2018). In this continental sedimentary record, the volcanic ash-fall deposits that have been preserved as tuffs and tonsteins layers. Throughout the European C–P basins, such levels have been commonly used as marker beds owing to their instantaneous deposition (e.g. Bouroz *et al.* 1972; Paquette 1980). The common occurrence of zircon grains in tonsteins suitable for U–Pb radioisotopic dating has allowed calibration of biostratigraphy, as well as intra- and inter-basinal correlations (Bruguier *et al.* 2003; Michel *et al.* 2015; Laurent *et al.* 2017; Pellenard *et al.* 2017; Ducassou *et al.* 2019).

Chronostratigraphy of Carboniferous-Permian continental basins of intertropical eastern Pangaea

C–P sedimentary successions of the western European basins are divided into regional stages, referred to in chronological order as Westphalian, Stephanian, Autunian, Saxonian, Thuringian or Rotliegend, and Zechstein (e.g. Menning *et al.* 2006; McCann 2008; Aretz *et al.* 2020; Henderson *et al.* 2020). The chronostratigraphic framework of these C–P basins has long been based on lithostratigraphy and/or faunal and floral biozones, including macrofloras and palynomorphs (e.g. Doubinger 1974; Clayton *et*

al. 1977). However, the phyto-biogeography is also controlled by climate conditions and depositional environments. This has been documented, for instance, in the case of hygrophile and mesoxerophile floras, which have been used to define the Stephanian and Autunian stages, but are more likely to reflect the geographical distribution of the taxa driven by the water availability rather than an evolutionary trend (Becq-Giraudon *et al.* 1995). It is therefore possible to find 'persistent' Stephanian floras in the Autunian facies, or even to see incursions of Autunian floras into strata attributed to the Stephanian, as shown in the French Decazeville, Decize–La Machine and Blanzy–Le Creusot basins (Langiaux 1984; Broutin 1986; Broutin *et al.* 1990, 1999). In the Aumance Basin, specifically, the acknowledged Stephanian–Autunian boundary is based on sedimentological and stratigraphic (discontinuity) criteria, preventing any correlation with other basins (Becq-Giraudon *et al.* 1995). The only case of a precise definition of the Carboniferous–Permian boundary in the western Europe C–P basins in correspondence with the macroflora biozonation and the Stephanian–Autunian boundary is in the Autun Basin, as determined by precise CA–ID–TIMS U–Pb geochronology of tonsteins (Pellenard *et al.* 2017; Aretz *et al.* 2020). The case of the Saxonian continental stage is even more controversial, as it has been described as aphytic and azoic, which would reflect taphonomic preservation biases rather than an actual disappearance of taxa. Therefore, these historical continental subdivisions may have diachronous boundaries, preventing reliable correlation to the Standard Global Chronostratigraphic Chart (SGCS) and therefore are rarely suitable for absolute geochronology and correlation purposes (Becq-Giraudon *et al.* 1995; Broutin *et al.* 1999; Mercuzot *et al.* 2021a), hence requiring numerical ages obtained through independent isotopic chronometers.

The French Massif Central Carboniferous to Permian basins

The French C–P basins crop out in the vicinity of the Variscan magmatic and metamorphic massifs (e.g. Armorican and Vosges massifs, Alps and Massif Central, Fig. 1) and are attributed to the syn- to late-orogenic extension and concomitant exhumation of high-grade metamorphic domes (e.g. Faure *et al.* 2009; Cochelin *et al.* 2021). The C–P basin strata occur in scattered outcrops with limited areal distribution (several tens of km^2), but they also underlie the sedimentary cover of the main Meso-

Cenozoic basins (i.e. Paris, Aquitanian and SE basins), where they can reach several hundred of km^2 (Beccaletto *et al.* 2015). Recently, Mercuzot *et al.* (2021a, 2022) suggested that the original extent of the present-day basins was significantly larger, raising the idea that (i) these basins could have been connected together at the time of their infilling, and (ii) that the subsurface basins represent the lateral extension of the exposed basinal strata (Beccaletto *et al.* 2015). Consequently, the present disparate exposures may represent preserved depocenters of the larger basins.

The Autun, Aumance, Decize–La Machine and Blanzy–Le Creusot basins of the NE Massif Central (Fig. 1) are mostly filled with fine- to coarse-grained siliciclastic sediments, which have been attributed to four main depositional environments: fluvial, palustrine, deltaic and lacustrine (e.g. Paquette 1980; Marteau 1983; Mathis and Brulhet 1990; Donsimoni 1990; Ducassou *et al.* 2019; Mercuzot *et al.* 2021a, 2021b, 2022). Recent chemostratigraphic analyses of the Autun Basin have revealed episodic wet intervals of short duration (about 10^5 yr, Garel *et al.* 2017; Mercuzot *et al.* 2021b), hence difficult to correlate across the neighbouring basins without any precise chronostratigraphic scheme. A substantial amount of volcanogenic material is found interbedded with the basinal sedimentary successions, either as volcanoclastic deposits or as volcanic flows and volcanic ash layers (i.e. tonsteins). Some tonsteins have been the subject of CA–ID–TIMS U–Pb analyses in the Autun Basin, giving depositional ages ranging from 299.91 ± 0.38 Ma to 298.05 ± 0.39 Ma (2-σ uncertainties) in the lower half-part of the sedimentary succession (Pellenard *et al.* 2017). In the Decize–La Machine Basin, zircon grains extracted from tonsteins gave consistent, though less precise, ages through LA–ICP–MS analyses, ranging from 299 ± 2 Ma to 295 ± 5 Ma (2-σ uncertainties, Ducassou *et al.* 2019). No absolute age constraints are presently available from the neighbouring Aumance Basin.

The Decize–La Machine Basin (Lucenay-lès-Aix Area). The Decize–La Machine C–P Basin partially crops out adjacent to the La Machine Village (La Machine Horst, Fig. 1b), while the main body of the sedimentary succession (surrounding the horst) is buried under the 60 to 370 m thick Meso-Cenozoic sedimentary cover of the southern Paris Basin (Fig. 1a), with a minimal extension of 50 km². The southern subsurface part, referred to the Lucenay-lès-Aix Area, has been recently studied using drill-

cores, well-logs and seismic profiles, in order to re-evaluate the chronostratigraphic framework and depositional setting of the basin (Ducassou *et al.* 2019; Mercuzot *et al.* 2021a, 2021b). The complete C–P sedimentary succession in the Lucenay-lès-Aix Area (Fig. 2a) is about 1000 m thick and is divided from base into four formations, namely the La Machine, Lucenay, Grey Autunian and Red Permian formations (Fig. 2a), which were deposited between about 301 and 290 Ma, based on preliminary LA–ICP–MS U–Pb geochronology (Ducassou *et al.* 2019). The depositional setting was dominated by deltaic and lacustrine environments and marginal-lacustrine floodplains (swamps), where coal deposits accumulated. Siliciclastic sediments with a significant volcanogenic component were deposited in alluvial-fan deltas within lakes or swamps. Frequent tonstein and lahar levels intercalated in swamps deposits were found in mines and boreholes (Donsimoni 1990; Ducassou *et al.* 2019; Mercuzot *et al.* 2021a). A 593 m long borehole named LY–F (46.71872301°N; 3.49736547°E) was drilled in the Decize–La Machine Basin, 2 km north of the Lucenay-lès-Aix Village (Fig. 1b). The recovered core comprises several centimetre to decimetre thick tonstein layers occasionally intermixed with reworked clastic material (Ducassou *et al.* 2019).

The Aumance Basin. The Aumance Basin is located 30 km westwards of the Decize–La Machine Basin, with a surface exposure of approximately 400 km² (Fig. 1b). In its northern part, the sedimentary successions are covered by the Meso-Cenozoic units of the Paris Basin. The subsurface depocenters are known as the Contres, Brécy and Arpheuilles sub-basins and probably correspond to a wider C–P basin (Beccaletto *et al.* 2015). The exposed succession is up to 1000 m thick and is made up of siliciclastic and volcanoclastic deposits, representing floodplain, delta, lake and fluvial environments, similar to those described in the Lucenay-lès-Aix Area (Paquette 1980; Bonnion 1983; Debriette 1985; Paquette and Feys 1989; Mathis and Brulhet 1990). The succession is subdivided into four main lithostratigraphic formations, namely the Inférieure, Mouillère, Buxières and Renière formations, ranging from the Stephanian to the upper Autunian continental stages and is overlain by a Saxonian Unit (Fig. 2b). In the upper part of the Buxières Formation, a plurimetric coal seam, referred to as the "Couche du Toit" (Fig. 2b), is overlain by a plurimetre thick oil-shale bed containing several tonstein layers. Two of these

tonsteins with centimetre-scale thicknesses referred to as "Lien Blanc" (white) and "Lien Vert" (green), form remarkably continuous marker beds across the basin. However, no published ages exist for these two tonstein layers, preventing inter-basinal correlations. The occurrence of these tonsteins also coincides with the deposition of the "Meiller Quartzites", corresponding to thick hydrothermal siliceous sinter (chalcedony), interbedded with the dominantly clastic sediments and interpreted as resulting from high volcanic activity in this area (Marcoux *et al.* 2004; Debriette and Legrand 2021).

Samples and methods

Samples. In the studied sedimentary successions, tonsteins occur as centimetre to decimetre thick clay-rich levels, often distinguished with sharp boundaries and paler colours (whitish, greenish or beige) relative to their enclosing sediments; they exhibit soapy texture in drill cores. Three tonstein samples were selected from the Decize–La Machine and Aumance basins for U–Pb analyses by CA–ID–TIMS at the Massachusetts Institute of Technology (MIT) Isotope Laboratory. Two samples were collected from the LY–F drill-core in the Decize–La Machine Basin (LYF-567.7 sample in the Lucenay Formation, and LYF-416.5 sample in the Grey Autunian Formation, Fig. 2a), and one sample from the Aumance Basin, in the Buxières Formation, corresponding to the "Lien Vert" tonstein (LV sample, Fig. 2b).

Methods. To reliably identify tonsteins containing autocrystic (unreworked) zircon grains, a series of investigations was undertaken prior to the U–Pb analyses. Mineralogical and geochemical analyses were first performed to verify the primary magmatic (ash fall) origin of the selected tonsteins, respectively at the Biogeosciences Laboratory (Université de Bourgogne–Franche-Comté, France) and at the SARM (CRPG-CNRS, Nancy, France). As volcanic rocks from the C–P basins commonly comprise xenocrystic zircon grains that can be significantly older than the age of volcanic eruption (e.g. Hoffmann *et al.* 2013; Michel *et al.* 2015; Ducassou *et al.* 2019; Lützner *et al.* 2021), we performed preliminary geochronological analyses by the LA–ICP–MS method on the LV sample at the Géosciences Rennes Laboratory (Université de Rennes 1, France), and used the published LA–ICP–MS age results of the

LYF-416.5 and LYF-567.7 samples of Ducassou *et al.* (2019) in order to guide zircon grain selection from the LY–F drill-core samples.

Mineralogical investigations

Mineralogical analyses by X-Ray Diffractometry (XRD) were performed to assess the volcanogenic nature of the collected samples, by ensuring the dominance of neoformed, well-crystallized kaolinite, or mixture with random or regular illite-smectite mixed-layers (i.e. IS R1, Bohor and Triplehorn 1993; Spears 2012; Pellenard *et al.* 2017), consistent with local burial diagenesis (low to moderate vitrinite reflectance, up to 0.59%, Donsimoni 1990). Epiclastic deposits (i.e. contaminated by detrital particles) were suspected in case of detection of illite, chlorite, or other mixed-layer clays such as chlorite-vermiculite. The mineralogical analyses of samples from the Lucenay-lès-Aix Area were performed by Ducassou *et al.* (2019), while the LV sample from the Aumance Basin was analyzed in the present study. The whole-rock samples were manually powdered in an agate mortar and analyzed on a D4 Endeavor diffractometer (Bruker AXS), with CuKα radiation and equipped with a LynxEye detector and a Ni filter under a 40 kV-25 mA current, at the Biogeosciences Laboratory (GISMO analytical platform, Université de Bourgogne, France). Then, the clay fraction (< 2 µm) was isolated and analyzed following the Holtzapfel (1985) and Moore and Reynolds (1997) protocols: chemical treatment with a 0.2 M hydrochloric acid (HCl) solution to dissolve potential carbonates, followed by successive rinses until reaching a neutral pH allowing the clay minerals to defloculate. After complete agitation and rinsing for 1.5 hours, the clay fraction in suspension in the upper two centimetres of the supernatant was withdrawn, then concentrated by centrifuging (2500 rpm for 40 minutes) and spreading on glass slides. Three separate runs on the diffractometer were carried out to identify the clay mineralogy: 1) after air-drying, 2) after dissolution in ethylene-glycol, and 3) after heating at 490°C for 2 hours. Semi-quantitative mineralogical compositions were obtained from diffractograms, based on the measured areas of the peaks corresponding to the principal reflections of the 001 crystal planes, which were calculated using the MacDiff 4.2.5 software (Petschick 2001).

Whole rock geochemistry

To complement XRD mineralogical analyses and to provide insights into the nature and source of volcanism, we analyzed the major and trace element geochemical composition of tonsteins. Samples were hand-crushed in an agate mortar and major and trace elements were then analyzed after alkaline fusion by Inductively Coupled Plasma–Optical Emission Spectrometry (ICP–OES) and Inductively Coupled Plasma–Mass Spectrometry (ICP–MS) at the SARM (CRPG-CNRS, Nancy, France), following the procedure of Carignan *et al.* (2001). Analytical results of samples from the Decize–La Machine Basin are already presented in Ducassou *et al.* (2019); complete analytical data are provided in the Supplementary Material Table 1.

U–Pb zircon geochronology

The zircon grains were extracted through conventional heavy mineral separation procedures, handpicked under a binocular microscope, embedded in epoxy resin mounts and polished, to expose the equatorial cross-sections of the grains. The grains were imaged by cathodoluminescence (Reliotron CL system equipped with a digital colour camera) to identify core-rim relationships and internal zoning patterns. In order to screen samples for xenocrystic and/or reworked zircon grains prior to CA–ID–TIMS analyses, preliminary U–Pb analyses were performed on all three samples by the LA–ICP–MS method. Detailed analytical data are listed in the Supplementary Material Table 2. Between 40 and 95 grains per sample were selected for *in situ* LA–ICP–MS analyses, using an Agilent 7700x quadrupole ICP–MS linked to an ESI NWR193UC Excimer 193 nm wavelength laser source, at the GeOHeLiS platform (Géosciences Rennes Laboratory, Université de Rennes 1, France), following the methodology described in Nosenzo *et al.* (2022). Analytical data are provided in the Supplementary Material Table 3.

For each sample, five concordant zircon grains identified by LA–ICP–MS were dislodged from the grain mounts and analyzed by the CA–ID–TIMS method at the Massachusetts Institute of Technology (MIT) Isotope Laboratory, following the procedures outlined in Ramezani *et al.* (2022). Selected zircon grains

were annealed at 900ºC for 60 hours in a muffle furnace, followed by partial dissolution in purified 29 M HF at 210ºC for 12 hours inside a high-pressure vessel, using methods modified after Mattinson (2005). Chemically abraded grains were fluxed successively in 3.5 M HNO_3 and 6 M HCl on a hot plate and in an ultrasonic bath and thoroughly rinsed after each step with purified water to remove the leachates. Zircon grains were then loaded individually into PFA microcapsules, spiked with the EARTHTIME ET535 mixed ^{205}Pb–^{233}U–^{235}U tracer solution (Condon *et al.* 2015; McLean *et al.* 2015), and completely dissolved in 29 M hydrofluoric acid (HF) at 210ºC for 48 hours. Dissolved Pb and U were purified by an HCl-based anion exchange column chemistry procedure (Krogh 1973), loaded together onto an outgassed Re filament in a silica gel/phosphoric acid mixture. Ratios of U and Pb isotopes were measured on an IsotopX X62 multi-collector thermal ionization mass spectrometer equipped with a Daly photomultiplier ion counting system at MIT. Pb isotopes were measured as mono-atomic ions in a peak-hopping mode on the ion counter, and were corrected for mass-dependent isotope fractionation by applying an independently determined fractionation correction of 0.18% ± 0.05% per atomic mass unit (2σ). U isotopes were measured as dioxide ions in a static mode using three Faraday collectors, while subjected to a within-run mass fractionation correction using the $^{233}U/^{235}U$ ratio of the tracer and a sample $^{238}U/^{235}U$ ratio of 137.818 ± 0.045 (Hiess *et al.* 2012), as well as an oxide correction based on an $^{18}O/^{16}O$ ratio of 0.00205 ± 0.00005.

A total of 15 single zircon grains from three samples were analyzed; complete analytical data are provided in the Supplementary Material Table 4. Data reduction, calculation of dates and propagation of uncertainties used the Tripoli and ET_Redux applications and algorithms (Bowring *et al.* 2011; McLean *et al.* 2011). The measured $^{206}Pb/^{238}U$ dates were corrected for initial ^{230}Th disequilibrium based on a magma Th/U ratio of 2.8 ± 1.0 (2σ). The age for each tonstein was calculated based on the weighted mean of its $^{206}Pb/^{238}U$ dates, after excluding outliers identified as xenocrysts (only one instance: Zr 031 of the LYF-416.5 sample, Supplementary Material Table 4). Uncertainties on the weighted mean dates are reported at 95% confidence interval and in the ± *X*/*Y*/*Z* Ma format, where *X* is the internal error based on analytical uncertainties only, *Y* includes the added tracer calibration uncertainty, and *Z* includes *Y* plus the ^{238}U decay constant uncertainty of Jaffey *et al.* (1971). *Y* should be considered when comparing

dates with those derived from other U–Pb methods (e.g. LA–ICP–MS) or with those using a different isotopic tracer.

Bayesian age-depth modelling

A non-parametric probabilistic age-depth model was constructed for the middle interval of the LY–F drill-core, based on the new CA–ID–TIMS ages and using the Bayesian interpolation algorithm of the Bchron R software package (Haslett and Parnell 2008; Parnell *et al.* 2008). This model requires at least two independently dated levels, assumes a normal distribution for the input weighted mean $^{206}Pb/^{238}U$ dates, follows the principle of stratigraphic superposition, and is based on random variability in sediment accumulation rates. The advantage of this age-depth model over conventional linear extrapolation or spline-fit methods is that it takes into account possible changes in sediment accumulation rate as a function of depositional gaps or lithological variability.

Results

Identification of ash-fall deposits

Mineralogy. Mineralogical results of the whole-rock and clay fraction are presented in Table 1. In the three analyzed samples, the bulk-rock comprises clay minerals, quartz, carbonates (including dolomite and siderite), apatite, feldspars, goethite, pyrite and gypsum.

The LV sample of the Aumance Basin is dominated by 37% quartz, followed by 28% carbonates (mainly dolomite), 28% clay minerals, and 7% apatite, feldspars, goethite and pyrite (Fig. 3a, Table 1). In the clay-size fraction, regular illite-smectite R1-type mixed-layer (i.e. rectorite) is the dominant clay mineral (52%), followed by kaolinite (48%) (Fig. 3b, Table 1). Results for the Lucenay-lès-Aix Area in the Decize-La-Machine Basin are detailed in Ducassou *et al.* (2019) and briefly summarized here: the whole-rock semi-quantitative mineralogy for the LYF-567.7 and LYF-416.5 samples exhibits a dominance of the clay minerals (54 and 56%, respectively), followed by quartz (37 and 12%, respectively). The other minerals are minor, yet with a non-negligible proportion of goethite and gypsum in the LYF-416.5 sample (16 and 13%, respectively). In the clay fraction, kaolinite is the main mineral

(75 and 88%, respectively), followed by IS mixed-layers (17 and 12%, respectively). Quartz is also present in the clay fraction in the LYF-567.7 sample (8%), while absent from the LYF-416.5 sample. For each of these samples, the dominance of well-crystallized kaolinite and IS R1 mixed-layer clay minerals confirm a volcanic origin (Spears 1970, 2012; Königer and Stollhofen 2001; Pellenard et al. 2017), while the absence of mica/illite suggests a low contamination of these levels by detrital material, either through mixing with inherited particles (i.e. incorporation of minerals from soils or metamorphic or magmatic basement during reworking or volcanic eruption), or reworking of the enclosing detrital lithologies during or after the deposition, thus making these tonsteins good candidates for zircon geochronology.

Geochemical composition. Geochemical data for the Decize–La Machine Basin samples LYF-567.7 and LYF-416.5 published in Ducassou *et al.* (2019) have been complemented with the LV sample from the Aumance Basin, and can be found in the Supplementary Material Table 1. These data are presented in chemical diagrams of immobile trace and REE elements, adapted to the study of volcanic-ash samples because of their good preservation (e.g. Bohor and Triplehorn 1993; Wray 1999; Huff 2016). Although single tonstein samples may not be fully representative of the magma composition, samples from both the Aumance and Decize–La Machine basins exhibit broad similarity to an intermediate rhyodacitic/dacitic composition on the discrimination plot of Winchester and Floyd (1977) (Fig. 4a). Shale-normalized REE profiles show a pronounced negative Eu anomaly, more marked in the LV sample (Fig. 4b), which is characteristic of plagioclase fractionation in magma and is commonly observed in the chemical composition of tonsteins derived from felsic volcanism (Bohor and Triplehorn 1993; Spears 2012; Pellenard *et al.* 2013, 2017).

U–Pb geochronology

Zircon characterization. Characterization of the aAnalyzed zircons from the LY-F samples have been described in Ducassou et al. (2019). From the LV sample, a total of 375 predominantly euhedral and prismatic zircon grains have been extracted, ranging in length from 20 to 330 µm and with a bimodal

distribution centred around 45 and 90 µm. Ninety-five zircon grains with typical magmatic zoning and free of xenocystic cores in their CL images were analyzed by LA–ICP–MS.

LA–ICP–MS method. Detailed analytical LA–ICP–MS results are summarized in Table 2; all ages are reported with 95% confidence level internal uncertainties. On a Tera-Wasseburg diagram, the LV analyses range from concordant to discordant without defining any simple trend (Fig. 5a). The concordant data spread along the concordia curve between 267.1 ± 2.5 Ma and 303.8 ± 3.4 Ma (Fig. 5b); discordant analyses are consistent with common lead contamination and/or lead loss. Detailed analytical results for samples LYF-567.7 and LYF-416.5, providing ages of 299.0 ± 2 Ma and 298.0 ± 4 Ma, respectively, are presented in Ducassou *et al.* (2019) and Table 2. Complete LA–ICP–MS Pb and U isotopic data for the LV sample is provided in Supplementary Materials Table 3.

CA–ID–TIMS method. A total of 15 zircon grains from the 3 tonstein samples were dislodged from epoxy mounts for CA–ID–TIMS analyses, while preference was given to concordant zircon grains with the youngest measured LA–ICP–MS ages. In cathodoluminescence, these grains show oscillatory zoning typical of magmatic zircon grains (Fig. 6). The objective was to overcome the effects of Pb loss through the chemical abrasion pre-treatment, in order to obtain the youngest population of accurate analyses. The results are presented in Figure 7 and summarized in Table 2, and the complete U–Pb isotopic data are provided in Supplementary Materials Table 4.

All analyses from the respective samples overlap within analytical uncertainty and define statistically coherent clusters from which a weighted mean $^{206}Pb/^{238}U$ age can be calculated without excluding any outliers. The only exception was an imprecise analysis associated with a small zircon grain (Zr 031) from sample LYF-416.5, which yielded a slightly older date of 300.6 ± 1.3 and was excluded from age calculation. The three calculated ages are 298.592 ± 0.075/0.15/0.35 Ma for the LV sample, with a mean square weighted deviation (MSWD) of 0.32 (Fig. 7a), 298.73 ± 0.11/0.17/0.36 Ma (MSWD = 0.34) for LYF-416.5 (Fig. 7b), and 299.111 ± 0.076/0.15/0.35 Ma (MSWD = 0.99) for LYF-567.7 (Fig. 7c). The compositional purity of the tonsteins, as well as the consistency of their zircon dates, suggest that the

calculated ages represent the timing of volcanic eruption and serve as a good approximation for the age of sedimentary deposition.

Age-depth model. The Bayesian age-depth model for the lower LY–F well based on the two tonstein U–Pb CA–ID–TIMS ages of this study yields an interpolated age of 298.80 +0.17/-0.12 Ma for the top of the Lucenay Formation, which coincides with the Stephanian–Autunian boundary (95% confidence interval, Fig. 8). The two ages obtained from the LY-F core delimit an interval of 151.10 m (compacted sediments) between LYF-567.7 (basal Lucenay Formation) and LYF-416.5 samples (lower Grey Autunian), allowing to calculate an average (compacted) sediment accumulation rate of 453 ± 159 m/Myr.

Discussion

Reassessment of the local-scale basinal chronostratigraphic framework

The new CA–ID–TIMS geochronology from the Decize–La Machine Basin is capable of resolving the ages of the two analyzed tonsteins outside their respective uncertainties, which was not possible based on the previously reported LA–ICP–MS data (Fig. 2). This allows significant enhancement to the age framework of the Lucenay and Grey Autunian formations, as originally established by Ducassou *et al.* (2019) (Fig. 9).

In the Aumance Basin, Marcoux *et al.* (2004) reported a U–Pb SHRIMP age of 300 ± 21 Ma from hydrothermal zircon grains associated with gold-bearing siliceous sinter deposits within the Autunian sedimentary succession (Fig. 2b). Together with biostratigraphic data, this age was used to attribute the Buxières Formation (Aumance Basin) to the early Artinskian Stage (Fig. 9, Schneider and Werneburg 2006; Schneider *et al.* 2020). However, the new and precise age for the "Lien Vert" tonstein (i.e. LV sample, 298.592 ± 0.075/0.15/0.35 Ma), while broadly consistent with the "Meiller Quartzites" age considering the large uncertainty of the latter, is substantially more precise and now places the Buxières Formation close to the Carboniferous-Permian boundary, with an overall deposition either in the latest Gzhelian Stage (latest Carboniferous Period) or the earliest Asselian Stage (earliest Permian Period)

considering analytical uncertainty (Fig. 2b). The new CA–ID–TIMS results therefore shifts by about 10 Ma the age of the Buxières Formation. In the absence of any other radioisotopic age data from the Aumance Basin, the lower and upper limits of the Buxières Formation or other formations of this basin cannot be precisely constrained, as illustrated in Figure 9. The new U–Pb geochronology also indicates that the evolution of the Decize–La Machine and the Aumance basins was at least partially simultaneous.

Palaegeographical implications

The NE Massif Central comprises various C–P basins (Fig. 1b), including the Decize–La Machine, Aumance, Autun, and Blanzy–Le Creusot basins, as well as the associated C–P successions that underlie the Meso-Cenozoic sedimentary cover of the Paris Basin to the north (Fig. 1a, Contres, Arpheuilles and Brécy basins). All these basins formed during the late- to post-orogenic extensional Variscan stages and are located southwards of the Variscan Front and the Eo-Variscan Suture (Fig. 1a, e.g. Ménard and Molnar 1988). Previous studies suggested that the presently exposed sedimentary successions correspond to partially preserved depocenters of ancient, more extensive sedimentary domains. This hypothesis is based on subsurface and sedimentological evidence, such as present-day erosional borders, palaeogeography, and significant post-early Permian erosion (Beccaletto *et al.* 2015; Mercuzot *et al.* 2021a, 2022). Accordingly, possible interconnections between western Europe basins during the late Carboniferous and the early Permian periods have been proposed, especially in reference to palaeobiogeography of elasmobranchs (freshwater sharks, and actinopterygians), including specimens from the Buxières Formation of the Aumance Basin (Poplin 1999; Schneider and Zajíc 1994; Schneider *et al.* 2000). Recent palaeontological and palaeobiogeographical data on actinopterygians (Štamberg and Steyer 2021) and on *Orthacanthus* species (freshwater shark, Luccisano *et al.* 2022) also confirm connections during the Permian Period between various basins located in France and Germany, including the Aumance and Autun basins (Luccisano *et al.* 2022). As the Decize–La Machine Basin is located in between the Aumance and Autun basins, this suggests that the Decize–La Machine Basin was also connected to the latter two. Specifically, specimens of *Orthacanthus kounoviensis* were found both

in the Buxières Formation of the Aumance Basin (close to the level of "Lien Vert" tonstein) and the Muse Formation of the Autun Basin (Muse oil-shale bed, Luccisano *et al.* 2022). Recent CA–ID–TIMS U–Pb geochronology of two tonsteins from the Muse oil-shale bed by Pellenard *et al.* (2017) provided ages of 298.05 ± 0.19/0.24/0.39 Ma and 298.57 ± 0.16/0.22/0.38 Ma. These ages are comparable to those presented here from the Aumance and Decize–La Machine basins (Figs. 2, 9, Table 2). This high-resolution and direct correlation indicates that (i) there is at least partial age overlap among the Buxières Formation (Aumance basin), the Muse Formation (Autun Basin) and the Lucenay and Grey Autunian formations (Decize–La Machine Basin), and (ii) the contemporaneous presence of *Orthacanthus kounoviensis* specimens in both the Autun and Aumance basins, and therefore the connection among the NE Massif Central basins close to the C–P boundary, are supported by independent U–Pb geochronology. It is also worth mentioning that the C–P biostratigraphy of insects and amphibians relies in part on specimens from the Aumance Basin (e.g. Schneider *et al.* 2020). The revised age of the Buxières Formation, based on the new "Lien Vert" tonstein age, therefore invites a re-evaluation of the biostratigraphy of these two clades, but is beyond the scope of the present study.

Implications of the new age constraints on the European chronological setting

The new ages from the Aumance and Decize-La-Machine basins indicate that the infilling of these basins occurred during the latest Carboniferous and the early Permian periods (Fig. 9). In addition, the age-depth modelling for the Decize-La-Machine Basin suggests that the boundary between the Lucenay and the Grey Autunian formations has an age of 298.80 +0.17/-0.12 Ma. This age is consistent with the global C–P boundary age of 298.92 ± 0.19 Ma (Ramezani *et al.* 2007), 298.90 ± 0.15 Ma (Schmitz and Davydov 2012) or 298.9 ± 0.4 Ma (Henderson *et al.* 2020), based on the CA–ID–TIMS U–Pb geochronology of the southern Urals stratotype.

The new geochronological results obtained in this study allow for inter-basinal correlations at both local and regional scales, which has been the subject of extensive work for the last decades, based on combined biostratigraphic and radioisotopic correlations (e.g. Roscher and Schneider 2005; Schneider and Scholze 2018; Schneider *et al.* 2020). These results indicate that the infilling of the Aumance and

Decize-La-Machine basins was contemporaneous with those of various basins across the Variscan Belt. Based on CA–ID–TIMS method, these include the Autun Basin (Pellenard *et al.* 2017), the Bohemian Czech Republic basins, where the Klobuky Coal tonstein in the Líně Formation of the Kladno-Rakovník Basin is dated at 298.97 ± 0.36 Ma (Opluštil *et al.* 2016a, Fig. 9), the Saar Nahe Basin in Germany, with an age of 298.7 ± 0.4 Ma from the Altenglan Formation, Glan Subgroup (Voigt *et al.* 2022), and the Thuringian Forest Basin, with a U–Pb age of 299.3 ± 0.3 Ma from the Ilmenau Formation (Lützner *et al.* 2021, Fig. 9). Our geochronological results from the Aumance Basin substantially modifies the biostratigraphy-based age of the Thuringian Forest Basin by about 16 Ma (Lützner *et al.* 2021). Previous SHRIMP U–Pb geochronology from the German basins are also consistent with our newly-acquired ages. The former includes ages of 296.6 ± 3.0 Ma (Planitz Formation) and 296 ± 3.0 Ma (Unkersdorf Formation), respectively, from the Chemnitz and Döhlen basins (Hoffmann *et al.* 2013), and 301 ± 3 Ma from the Saale Basin (Wettin subformation, Breitkreuz *et al.* 2009).

Our geochronology also reveals differences in basin development and infilling histories along the Variscan Belt. Some of the basins located northwards of the Variscan Belt (including the NE Massif Central basins), and basins located southwards, in more internal zones of the belt (e.g. the southern Massif Central basins such as the Lodève and Saint-Affrique basins), have different infilling histories. The major differences involve the thickness and time-span of their preserved sedimentary successions, more developed in the Lodève and Saint-Affrique basins and covering longer period of time (i.e. either longer depositional history or better preservation), probably up to the late-early or middle Permian, based on geochronological data from Michel *et al.* (2015) and Poujol *et al.* (2023), as well as biostratigraphic data (e.g. Schneider *et al.* 2020). Their differences also involve sedimentary facies and depositional environments: in both northern and southern basins, the environments are represented by well-developed fluvial/deltaic-lake systems (Mercuzot *et al.* 2021a, 2022), but only in the southern basins, they grade upwards into shallower and finer-grained red beds (i.e. playa-lake and soils), due to climate and tectonic controls (e.g. Schneider *et al.* 2006; Pochat and Van Den Driessche 2011; Pfeifer *et al.* 2020). Available age constraints and biostratigraphic data for the Lodève Basin (Schneider *et al.* 2006, 2020; Michel *et al.* 2015) could indicate a hiatus of sedimentation in this basin, spanning from the

latest Carboniferous Period (top of the Gzhelian Graissessac Formation at ca. 303 Ma, Fig. 9) to the earliest Permian Period (base of the Asselian Usclas–St.-Privas Formation at ca. 296 Ma; Schneider *et al.* 2020, Fig. 9). However, the occurrence of such a hiatus in the Lodève Basin is uncertain, as some reported ages from this basin are debated (Fig. 9). Therefore, the northern Massif Central basins could either be correlated to the Graissessac Formation of the Lodève Basin, based on a U–Pb zircon age of 295.5 ± 5.1 Ma (Bruguier *et al.* 2003), and the synthesis of Schneider *et al.* (2006), or coincide with a hiatus in the Lodève Basin, that ranged from ca. 303 to 296 Ma, according to Schneider *et al.* (2020), and thus not having any time equivalent strata in the latter (Fig. 9). In the Saint-Affrique Basin, there is no age constraint for the deposits between the Carboniferous Period and the late-early Permian Period (Kungurian Stage, base of the Kungurian Dourdou Formation dated at 280.3 ± 2.6 Ma, Poujol *et al.* 2023), which could also be due to a depositional hiatus, given the relatively small thickness of sediments from that time interval. Therefore, the uncertainty in the chronostratigraphic frameworks of the Lodève and Saint-Affrique basins at the C–P transition currently prevents correlation of their sedimentary successions with those of the other C–P basins across the Variscan Belt.

Implications for the European continental stages and correlation to the non-marine Carboniferous-Permian time scale

Our interpolated age of 298.80 + 0.17/-0.12 Ma for the transition between the Stephanian and Autunian in the Decize–La Machine Basin may suggest that this transition is locally synchronous with the global C–P boundary. However, in this basin, the Stephanian-Autunian transition has been debated because it is based on lithostratigraphy and floral biostratigraphy (mostly on *Callipteris* species; Grangeon *et al.* 1968; Primey and Farjanel 1989), both of which may depend on palaeoenvironmental conditions. In the neighbouring Aumance Basin, about 40 km to the SW, the new "Lien Vert" tonstein age also overlaps with the C–P boundary. This suggests that the Buxières Formation, once considered as Sakmarian–Artinskian (Schneider and Werneburg 2006, Fig. 2a), possibly encompasses the C–P boundary. In addition, the underlying Mouillère and Inférieure formations, previously considered as Gzhelian to Sakmarian (Schneider and Werneburg 2006, Fig. 2a), were most likely deposited during the

Carboniferous (Fig. 9). Moreover, CA–ID–TIMS geochronological results from the Autun Basin, about 70 km to the east of the Decize–La Machine Basin, also suggest that the Stephanian–Autunian transition occurred during the Gzhelian Stage (Pellenard *et al.* 2017, Fig. 9), as already evidenced in the Central and Bohemian basins (Opluštil *et al.* 2016a, 2016b). Therefore, the already suspected diachronism of the Autunian and Stephanian subdivisions (e.g. Becq-Giraudon *et al.* 1995; Knight and Wagner 2014), documented at regional scale (Opluštil *et al.* 2022) could also occur at a local geographical scale, i.e. between the Aumance and Autun basins and the Decize–La Machine Basin, but cannot be completely proven considering that in the latter, this transition is not well characterized. In conclusion, the late Carboniferous–early Permian continental subdivisions (i.e. Stephanian A, B, C, lower/upper Autunian), when based solely on lithostratigraphic facies without strong biostratigraphic and/or accurate radioisotopic data, are highly questionable and insufficient for inter-basinal correlations, as previously mentioned by some authors (Becq-Giraudon *et al.* 1995; Broutin *et al.* 1999; Opluštil *et al.* 2022; Pfefferkorn 2023).

Sediment accumulation rates and basinal evolution

The new geochronology, together with the Bayesian stratigraphic-age model of the Decize–La Machine Basin, indicate that a substantial thickness of sediments was deposited close to the C–P boundary (i.e. 298.9 ± 0.4 Ma, Henderson *et al.* 2020). The average compacted sediment accumulation rate of 453 ± 159 m/Myr obtained in the LY–F core is significantly higher compared to other time-equivalent successions with high-resolution geochronology elsewhere in the world. For example, the calculated average compacted sediment accumulation rate for the paralic, coal-bearing Taiyuan Formation (ca. 299.7–298.2 Ma, Wu *et al.* 2021) in the Ordos Basin of North China is only 67 ± 29 m/Myr. The higher apparent rate in the LY–F core may indicate higher subsidence in the depocenter of the Decize-La-Machine basin, as evidenced by massive, alluvial, conglomeratic sediments (debris flow/slump deposits) deposited in a relatively short time in the Lucenay Formation (Ducassou *et al.* 2019). Moreover, the contribution of the volcanism to these high depositional rates should be considered, as the abundance of

volcanogenic materials in fan-delta deposits of the LY-F core has been documented by Ducassou et al. (2019).

For the neighbouring Autun Basin, using the ages and stratigraphic constraints given in Pellenard *et al.* (2017), the average compacted sediment accumulation rate between the Igornay and Muse formations is estimated between 136 and 199 m/Myr (considering age uncertainties), which is nearly half of that for the Lucenay-lès-Aix Area of the Decize–La Machine Basin. This differences in the sedimentation rates between the two basins may be explained by a lack of volcaniclastic-rich deposits in the Autun Basin, together with the dominance of finer-grained terrigenous lithologies in the latter, as the Autun Basin records much deeper subaquatic environments (Mercuzot *et al.* 2021a, 2022).

The relatively high sediment accumulation rates observed in the Autun (Pellenard *et al.* 2017) and Decize-La-Machine basins (this work) is consistent with them having a shorter depositional history than previously estimated. In addition, the accumulation rate calculated in the Decize–La Machine Basin compares well with those estimated for other time-equivalent C–P basins across the Variscan Belt. For example, based on high precision geochronological results, compacted sedimentation rates obtained in Bohemian basins range between 50 and 240 m/Myr (Oplustil *et al.* 2016a), reach about 430 m/Myr in the Lodève Basin (Michel *et al.* 2015), and about 400 m/Myr in the Thuringian Forest Basin (Lützner *et al.* 2021). This finding is in line with the identification of short-lived C–P basins with high accumulation rates along the Variscan Belt (Opluštil *et al.* 2016a; Lützner *et al.* 2021). Although this preliminary observation relies on sedimentary thicknesses uncorrected for compaction, it suggests that the C–P basins of the Variscan Belt formed under a relatively similar tectonic regime. Indeed, the geodynamic setting was controlled by the rapid collapse of the Variscan Belt, responsible for the thinning of the continental crust, and triggering at the surface the formation of sedimentary basins with high subsidence rates controlled by normal detachments and faults (Burg et *al.* 1994; Ménard and Molnar 1988; Averbuch and Piromallo 2012; Vanderhaeghe *et al.* 2020). It also indicates that these basins were tectonically active, with high levels of both sediment influx and accommodation, allowing for progradation of deltaic systems in balanced-filled to overfilled lake systems (Mercuzot *et al.* 2022). High sediment influx, together with the immature nature of the coarse-grained facies (Ducassou *et al.*

2019) also reflects proximity to coeval topographical reliefs. Beside the role of this terrigenous sediment influx in a post-orogenic setting, the influence of climate, that was likely relatively humid given that the basins were in equatorial position, remains to be reliably constrained.

Conclusions and perspectives

High-resolution U–Pb geochronology by the CA–ID–TIMS method on three tonstein levels collected from Carboniferous–Permian basins in the northern French Massif Central (Aumance and Decize–La Machine basins) provided ages close to the Carboniferous–Permian boundary, ranging from 299.11 ± 0.35 Ma to 298.59 ± 0.35 Ma. The results are consistent with other ages previously published from NE French Massif Central basins, and indicate substantially high sediment accumulation rates, implying shorter depositional histories than previously estimated. Together with sedimentological, structural and palaeobiogeographical evidence, the new chronostratigraphic framework points out to physical connections between the presently disparate basins during their infilling.

This work offers new perspectives on the Carboniferous–Permian basin evolution throughout the eastern equatorial Pangaea, with important biostratigraphic, palaeogeographical, geodynamic and climate implications, which necessitate further focused investigations: (i) high-resolution chronostratigraphic frameworks based on radioisotopic age data highlight new disparities in the established biostratigraphic zonation at the European scale, which call on revisions to the early Permian faunal and floral evolution histories, (ii) statistically robust age models based on high-resolution geochronology can identify local changes in sediment accumulation and/or depositional gaps and their possible inter-basinal correlations in connection to the Variscan geodynamics, and (iii) well-calibrated basin evolution histories would allow re-evaluation of local versus global climate signals, leading to a better understanding of the Earth system response to the demise of the LPIA.

Acknowledgements

The authors greatly thank Yves Paquette and Dominique Chabard for providing the “Lien Vert” sample from the Aumance Basin. They are also grateful to Pierre Debriette for the field excursion in the

Aumance Basin, as well as Georges Gand and Ludovic Bruneau for their assistance in the field and in the laboratory, respectively. The authors thank Michael A. Pointon and an anonymous reviewer who provided valuable comments, contributing significantly to the improvement of the original manuscript.

Author Contributions

MM, CR, SB, LB, PP: conceptualization; CR, JR, MP, CD: data curation; CR, JR, CD: formal analysis; MM, SB: funding acquisition; MM, CR, SB; CR, JR, MP, PP: validation; MM, CR, SB, JR: visualization; MM, CR: writing – original draft; MM, CR, SB, JR, MP, CD, LB, PP: writing – review and editing.

Funding information

This work was supported by the TelluS Program of CNRS/INSU.

Data availability statement

All data generated or analyzed during this study are included in this published article (and its supplementary information files).

Figure captions

Fig. 1. (a) Map of western Europe showing the main Variscan tectonic structures and the late Carboniferous to early Permian basins (Southern European Basin; modified from Beccaletto *et al.* 2015; Schneider and Scholze 2018), in both outcrop and in subsurface. (b) Distribution of the late Carboniferous to Permian basins of the NE Massif Central displaying the studied Aumance and Decize–La Machine basins, as well as the Lucenay-lès-Aix Area (modified from Elsass-Damon 1977). AM, Armorican Massif; MC, Massif Central; VM, Vosges Massif.

Fig. 2. Composite lithostratigraphic sections of (a) the Decize–La Machine Basin (Lucenay-lès-Aix Area) and (b) the Aumance Basin, along with the European continental stages (modified after Paquette

1980; Donsimoni 1990; Ducassou *et al.* 2019). LA–ICP–MS ages of the LY-F core are from Ducassou *et al.* (2019). The Aumance's hydrothermal sinters "*Meiller quartzites*" have been dated at 300 ± 21 Ma by sensitive high-resolution ion microprobe (SHRIMP) U–Pb analyses of hydrothermal zircon grains (Marcoux *et al.* 2004). OM, organic matter; Fm., Formation. Red stars mark newly analyzed tonstein levels.

Fig. 3. X-ray powder diffractograms for the LV tonstein from the Aumance Basin, including whole-rock (a) and clay-fraction (<2 μm) only (b). IS, regular illite-smectite mixed-layers (rectorite); d, lattice spacing.

Fig. 4. Geochemical ICP–MS and ICP–OES data for the three selected tonsteins. Data for LYF-567.7 and LYF-416.5 after Ducassou *et al.* (2019). (a) Zr/TiO2 vs Nd/Y diagram (Winchester and Floyd 1977) and (b) REE profiles normalized to the Cody-shale (Jarvis and Jarvis 1985).

Fig. 5. LA–ICP–MS concordia diagrams for the LV tonstein sample (Aumance Basin). The diagrams were generated using IsoplotR (Vermeesch 2018). Error ellipses are depicted at the 2σ level. (a). Tera-Wasserburg diagram showing all analyses. (b) Wetherill diagram focused on the concordant analyses (blue filled ellipses). Open ellipses correspond to discordant analyses.

Fig. 6. Cathodoluminescence images of representative zircon grains analyzed by LA–ICP–MS and CA–ID–TIMS. Uncertainties on $^{206}Pb/^{238}U$ dates are given at the 2σ level.

Fig. 7. Results of CA–ID–TIMS analyses shown in conventional concordia diagrams (left column) and ranked $^{206}Pb/^{238}U$ date plots (right column). (a) LV tonstein (Aumance Basin), (b) LYF-416.5 tonstein (Decize–La Machine Basin), (c) LYF-567.7 tonstein (Decize–La Machine Basin). Vertical bars are individual zircon analyses with their 2σ uncertainties; horizontal lines represent the calculated weighted mean $^{206}Pb/^{238}U$ age, and horizontal shaded band represents its 95% confidence interval internal

uncertainty (X). The age uncertainties are reported as ± *X/Y/Z* Ma (*X*: internal or analytical uncertainty in the absence of all external or systematic errors; *Y*: incorporating the U–Pb tracer calibration error; *Z*: including *X* and *Y*, as well as the *U* decay constant error).

Fig. 8. Bayesian age–depth model for the LY-F core (Decize–La Machine Basin, Lucenay-lès-Aix Area), based on CA–ID–TIMS geochronology of two tonsteins, LYF-567.7 and LYF-416.5, sampled 151.10 m apart in the LY-F core. The extrapolated age is in blue and constrains the boundary between the Stephanian (Lucenay Formation) and the Autunian (Grey Autunian Formation) continental stages.

Fig. 9. Correlation of the Carboniferous–Permian basins across western Europe based on available biostratigraphic and radioisotopic age constraints, upgraded with more recent radioisotopic data. Autun, Lodève (right column), Sardinian, Southern Italian Alps, Saar-Nahe basins and Thuringian Forest Basin (Tambach and Eisenach formations): Schneider *et al.* (2020), see references therein for detailed explanations; Decize–La Machine Basin: Ducassou *et al.* (2019) and this study; Aumance Basin: Schneider and Werneburg (2006) (left column) and this study (right column; the previously considered stratigraphic position of the "Lien Vert" tonstein is highlighted with a grey line); Thuringian Forest Basin (Möhrenbach to the Rötterode formations): Lützner *et al.* (2021).
Stars represent recent U–Pb geochronology: Autun Basin: Pellenard *et al.* (2017); Lodève Basin, left column: Bruguier *et al.* (2003) and Michel *et al.* (2015) (see Pochat and Van Den Driessche (2016) for an opposite view); Sardinian basins: Werneburg *et al.* (2007) and Gaggero *et al.* (2017); Southern Alps basins: Schaltegger and Brack (2007), Marocchi *et al.* (2008) and Berra *et al.* (2015); Saar Nahe Basin: Voigt *et al.* (2022); Thuringian Forest Basin: Lützner *et al.* (2021); Bohemian basins: Opluštil *et al.* (2016a). Lithological descriptions: Decize–La Machine Basin: Ducassou *et al.* (2019); Aumance Basin: Paquette (1980); Autun Basin: Mercuzot *et al.* (2022); Lodève Basin: Lopez *et al.* (2008); Sardinian basins: Ronchi *et al.* (2008), Gaggero *et al.* (2017); Southern Alps basins: Marocchi *et al.* (2008); Saar-Nahe Basin: Roscher and Schneider (2006); Thuringian Forest Basin: Lützner *et al.* (2021); Bohemian basins: Opluštil *et al.* (2013).

Table 1. Mineralogical compositions of the clay fraction and the bulk-rock for the LV (Aumance Basin), LYF-416.5 and LYF-567.7 (Decize–La Machine Basin) tonsteins, obtained using X-ray diffraction.

Table 2. LA–ICP–MS and CA–ID–TIMS ages for the three analyzed samples LV, LYF-416.5 and LYF-567.7.

Supplementary Material Table 1. ICP–MS and ICP–OES geochemistry results for the LV, LYF-416.5 and LYF-567.7 samples.

Supplementary Material Table 2. Operating conditions for the LA–ICP–MS equipment.

Supplementary Material Table 3. LA–ICP–MS results for the LV sample (Aumance Basin).

Supplementary Material Table 4. CA–ID–TIMS results for the LV, LYF-567.7 and LYF-416.5 samples.

References

Aretz, M., Herbig, H.G., Wang, X.D., Gradstein, F. M., Agterberg, F.P., Ogg, J. G. 2020. Chapter 23 - The Carboniferous Period. In: Gradstein, Felix M., Ogg, James G., Schmitz, M.D., Ogg, G.M. (eds) Geologic Time Scale 2020. Elsevier, 811–874, https://doi.org/10.1016/B978-0-12-824360-2.00023-1

Averbuch, O., Piromallo, C. 2012. Is there a remnant Variscan subducted slab in the mantle beneath the Paris basin? Implications for the late Variscan lithospheric delamination process and the Paris basin formation. Tectonophysics, 558, 70–83, https://doi.org/10.1016/j.tecto.2012.06.032

Beccaletto, L., Capar, L., Serrano, O., Marc, S. 2015. Structural evolution and sedimentary record of the Stephano-Permian basins occurring beneath the Mesozoic sedimentary cover in the southwestern Paris basin (France). Bulletin de la Société Géologique de France, 186, 429–450, https://doi.org/10.2113/gssgfbull.186.6.429

Becq-Giraudon, J.-F., Mercier, D., Jacquemin, H. 1995. Faut-il rassembler le Stéphanien supérieur et l'Autunien (Paléozoïque supérieur continental) en une seule entité lithostratigraphique ? Géologie de la France, 2, 17–24.

Benek, R., Kramer, W., McCann, T., Scheck, M., Negendank, J.F.W., Korich, D., Huebscher, H.-D., Bayer, U. 1996. Permo-Carboniferous magmatism of the Northeast German Basin. Tectonophysics, Dynamics of Extensional Basins and Inversion Tectonics, 266, 379–404, https://doi.org/10.1016/S0040-1951(96)00199-0

Berra, F., Tiepolo, M., Caironi, V., Siletto, G.B. 2015. U–Pb zircon geochronology of volcanic deposits from the Permian basin of the Orobic Alps (Southern Alps, Lombardy): chronostratigraphic and geological implications. Geological Magazine, 152, 429–443, https://doi.org/10.1017/S0016756814000405

Bishop, J.W., Montañez, I.P., Osleger, D.A. 2010. Dynamic Carboniferous climate change, Arrow Canyon, Nevada. Geosphere, 6, 1–34, https://doi.org/10.1130/GES00192.1

Bixel, F. 1988. Le volcanisme stéphano-permien des Pyrénées Atlantiques. Bulletin des centres de recherches exploration-Production Elf-Aquitaine, 12, 661–706.

Bohor, B.F., Triplehorn, D.M. 1993. Accretionary lapilli in altered tuffs associated with coal beds. Journal of Sedimentary Research, 54, 317–325.

Bonin, B. 1990. From orogenic to anorogenic settings: Evolution of granitoid suites after a major orogenesis. Geological Journal, 25, 261–270, https://doi.org/10.1002/gj.3350250309

Bonin, B., Brändlein, P., Bussy, F., Desmons, J., Eggenberger, U., Finger, F., Graf, K., Marro, Ch., Mercolli, I., Oberhänsli, R., Ploquin, A., von Quadt, A., von Raumer, J., Schaltegger, U., Steyrer, H.P., Visonà, D., Vivier, G. 1993. Late Variscan Magmatic Evolution of the Alpine Basement. In: von Raumer, J.F., Neubauer, F. (eds) Pre-Mesozoic Geology in the Alps. Springer, Berlin, Heidelberg, 171–201, https://doi.org/10.1007/978-3-642-84640-3_11

Bonin, B., Azzouni-Sekkal, A., Bussy, F., Ferrag, S. 1998. Alkali-calcic and alkaline post-orogenic (PO) granite magmatism: petrologic constraints and geodynamic settings. Lithos, 45, 45–70, https://doi.org/10.1016/S0024-4937(98)00025-5

Bonnion, S. 1983. Structuration du bassin houiller de l'Aumance(Allier) : analyse structurale des dépôts de charbon et stérile, géophysique. PhD thesis, Université de Dijon.

Bouroz, A., Roques, M., Vialette, Y. 1972. Etude de la cinérite au sommet de la zone 2 du bassin des Cévennes. Mémoires du BRGM, 77, 503–507.

Bowring, J.F., McLean, N.M., Bowring, S.A. 2011. Engineering cyber infrastructure for U-Pb geochronology: Tripoli and U-Pb_Redux. Geochemistry, Geophysics, Geosystems, 12, https://doi.org/10.1029/2010GC003479

Breitkreuz, C., Kennedy, A. 1999. Magmatic flare-up at the Carboniferous/Permian boundary in the NE German Basin revealed by SHRIMP zircon ages. Tectonophysics, 302, 307–326, https://doi.org/10.1016/S0040-1951(98)00293-5

Breitkreuz, C., Ehling, B.-C. Sergeev, S., 2009. Chronological evolution of an intrusive/extrusive system: the Late Paleozoic Halle Volcanic Complex in the northeastern Saale Basin (Germany). Zeitschrift der Deutschen Gesellschaft für Geowissenschaften, 173–190, https://doi.org/10.1127/1860-1804/2009/0160-0173

Broutin, J, 1986. Étude Paléobotanique et Palynologique du passage carbonifère permien dans le Sud-Ouest de la Péninsule Ibérique. Cahiers de paléontologie.

Broutin, J., Doubinger, J., Farjanel, G., Freytet, P., Kerp, H. 1990. Le renouvellement des spores au passage Carbonifère Permien : approches stratigraphique, biologique, sédimentologique. Comptes rendus de l'Académie des sciences. Série 2, Mécanique, Physique, Chimie, Sciences de l'univers, Sciences de la Terre, 311, 1563–1569.

Broutin, J., Chateauneuf, J.-J., Galt, J., Ronchi, A. 1999. L'Autunien d'Autun reste-t-il une référence pour les dépôts continentaux du Permien inférieur d'Europe ? Géologie de la France, 2, 17–31.

Bruguier, O., Becq-Giraudon, J.F., Champenois, M., Deloule, E., Ludden, J., Mangin, D. 2003. Application of in situ zircon geochronology and accessory phase chemistry to constraining basin development during post-collisional extension: a case study from the French Massif Central. Chemical Geology, 201, 319–336, https://doi.org/10.1016/j.chemgeo.2003.08.005

Burg, J.P., Van den Driessche, J., Brun, J.P. 1994. Syn-to post-thickening extension in the Variscan Belt of Western Europe: modes and structural consequences. Géologie de la France, 3, 33–51.

Carignan, J., Hild, P., Mevelle, G., Morel, J., Yeghicheyan, D. 2001. Routine analyses of trace elements in geological samples using flow injection and low pressure on-line liquid chromatography coupled to ICP-MS: a study of geochemical reference materials BR, DR-N, UB-N, AN-G and GH. Geostandards Newsletter, 25, 187–198, https://doi.org/10.1111/j.1751-908X.2001.tb00595.x

Cecil, C.B., DiMichele, W.A., Elrick, S.D. 2014. Middle and Late Pennsylvanian cyclothems, American Midcontinent: Ice-age environmental changes and terrestrial biotic dynamics. Comptes Rendus Geoscience, 346, 159–168, https://doi.org/10.1016/j.crte.2014.03.008

Chumakov, N.M., Zharkov, M.A. 2002. Climate during Permian–Triassic Biosphere Reorganizations, Article 1: Climate of the Early Permian. Stratigraphy and Geological Correlation, 10, 586–602.

Clayton, G., Coquel, R., Doubinger, J., Gueinn, K.J., Loboziak, S., Owen, B., Streel, M. 1977. Carboniferous miospores of Western Europe: illustration and zonation. Mededelingen-Rijks Geologische Dienst, 29.

Cloetingh, S.A.P.L., Ziegler, P.A., Bogaard, P.J.F., Andriessen, P.A.M., Artemieva, I.M., Bada, G., van Balen, R.T., Beekman, F., Ben-Avraham, Z., Brun, J.-P., Bunge, H.P., Burov, E.B., Carbonell, R., Faccenna, C., Friedrich, A., Gallart, J., Green, A.G., Heidbach, O., Jones, A.G., Matenco, L., Mosar, J., Oncken, O., Pascal, C., Peters, G., Sliaupa, S., Soesoo, A., Spakman, W., Stephenson, R.A., Thybo, H., Torsvik, T., de Vicente, G., Wenzel, F., Wortel, M.J.R. 2007. TOPO-EUROPE: The geoscience of coupled deep Earth-surface processes. Global and Planetary Change, 58, 1–118, https://doi.org/10.1016/j.gloplacha.2007.02.008

Cochelin, B., Lemirre, B., Denèle, Y., de Saint Blanquat, M. 2021. Strain partitioning within bending orogens, New insights from the Variscan Belt (Chiroulet-Lesponne domes, Pyrenees). Tectonics, 40, https://doi.org/10.1029/2020TC006386

Condon, D.J., Schoene, B., McLean, N.M., Bowring, S.A., Parrish, R.R. 2015. Metrology and traceability of U–Pb isotope dilution geochronology (EARTHTIME Tracer Calibration Part I). Geochimica Cosmochimica Acta, 164, 464–480, https://doi.org/10.1016/j.gca.2015.05.026

Copestake, P., Sims, A.P., Crittenden, S., Hamar, G.P., Ineson, J.R., Rose, P.T., Tringham, M. 2003. The Millennium Atlas: petroleum geology of the central and northern North Sea. Geological Society of London, 389.

Cortesogno, L., Cassinis, G., Dallagiovanna, G., Gaggero, L., Oggiano, G., Ronchi, A., Seno, S., Vanossi, M. 1998. The Variscan post-collisional volcanism in Late Carboniferous–Permian sequences of Ligurian Alps, Southern Alps and Sardinia (Italy): a synthesis. Lithos, 45, 305–328.

Davidson, J., Turner, S., Handley, H., Macpherson, C., Dosseto, A. 2007. Amphibole "sponge" in arc crust? Geology, 35, 787–790, https://doi.org/10.1130/G23637A.1

Debriette, P.J. 1985. Étude géologique du bassin permo-carbonifère de la Queune (Allier). PhD thesis, Université de Bourgogne.

Debriette, P., Legrand, P. 2021. Les quartzites de Meillers (Permien inférieur du bassin de Bourbon-l'Archambault, Allier, Massif central, France) : un élément du patrimoine géologique national. Revue des Sciences naturelles d'Auvergne, 85, 20.

Donsimoni, M. 1990. Le gisement de charbon de Lucenay-lès-Aix (Nièvre). Essai de synthèse géologique d'après les sondages récents (1981-1986). Editions du BRGM, Orléans, France.

Doornenbal, H., Stevenson, A. 2010. Petroleum geological atlas of the Southern Permian Basin area. EAGE.

Doubinger, J. 1974. Études palynologiques dans l'Autunien. Review of Palaeobotany and Palynology, Permian and Triassic Palynology, 17, 21–38, https://doi.org/10.1016/0034-6667(74)90089-X

Ducassou, C., Mercuzot, M., Bourquin, S., Rossignol, C., Pellenard, P., Beccaletto, L., Poujol, M., Hallot, E., Pierson-Wickmann, A.C., Hue, C., Ravier, E. 2019. Sedimentology and U-Pb dating of Carboniferous to Permian continental series of the northern Massif Central (France): Local palaeogeographic evolution and larger scale correlations. Palaeogeography, Palaeoclimatology, Palaeoecology, 533, 109228, https://doi.org/10.1016/j.palaeo.2019.06.001

Elsass-Damon, F. 1977. Les « schistes bitumineux » du bassin d'Autun : pétrographie, minéralogie, cristallochimie, pyrolise. PhD thesis, Université de Bourgogne.

Faure, M. 1995. Late orogenic carboniferous extensions in the Variscan French Massif Central. Tectonics, 14, 132–153, https://doi.org/10.1029/94TC02021

Faure, M., Lardeaux, J.-M., Ledru, P. 2009. A review of the pre-Permian geology of the Variscan French Massif Central. Comptes Rendus Geoscience, 341, 202–213, https://doi.org/10.1016/j.crte.2008.12.001

Fielding, C.R., Frank, T.D., Isbell, J.L. 2008. The late Paleozoic ice age—A review of current understanding and synthesis of global climate patterns. Resolving the Late Paleozoic Ice Age in Time and Space. Geological Society of America, 343–354, https://doi.org/10.1130/2008.2441(24)

Fisher, R.V., Schmincke, H.-U. 1984. Submarine Volcaniclastic Rocks. In: Fisher, R.V., Schmincke, H.-U. (eds) Pyroclastic Rocks. Springer, Berlin, Heidelberg, 265–296, https://doi.org/10.1007/978-3-642-74864-6_10

Fluteau, F., Besse, J., Broutin, J., Ramstein, G. 2001. The Late Permian climate. What can be inferred from climate modelling concerning Pangea scenarios and Hercynian range altitude? Palaeogeography, Palaeoclimatology, Palaeoecology, 167, 39–71, https://doi.org/10.1016/S0031-0182(00)00230-3

Foster, G.L., Royer, D.L., Lunt, D.J. 2017. Future climate forcing potentially without precedent in the last 420 million years. Nature Communications, 8, 14845, https://doi.org/10.1038/ncomms14845

Gaggero, L., Gretter, N., Langone, A., Ronchi, A. 2017. U–Pb geochronology and geochemistry of late Palaeozoic volcanism in Sardinia (southern Variscides). Geoscience Frontiers, 8, 1263–1284, https://doi.org/10.1016/j.gsf.2016.11.015

Garel, S., Behar, F., Schnyder, J., Baudin, F. 2017. Palaeoenvironmental control on primary fluids characteristics of lacustrine source rocks in the Autun Permian Basin (France). Bulletin de la Société Géologique de France, 188, 29, https://doi.org/10.1051/bsgf/2017187

Grangeon, M., Feys, R., Greber, C.H., Raymond, A.L. 1968. Géologie profonde de la région de Decize (Nièvre). Essai de synthèse d'après les sondages profonds. Bulletin du Bureau des Recherches Géologiques et Minières, 4, 43–108.

Haslett, J., Parnell, A. 2008. A simple monotone process with application to radiocarbon-dated depth chronologies. Journal of the Royal Statistical Society: Series C (Applied Statistics), 57, 399–418, https://doi.org/10.1111/j.1467-9876.2008.00623.x

Henderson, C.M., Shen, S.Z., Gradstein, F. M., Agterberg, F.P. 2020. Chapter 24 - The Permian Period. In: Gradstein, Felix M., Ogg, J.G., Schmitz, M.D., Ogg, G.M. (eds) Geologic Time Scale 2020. Elsevier, 875–902, https://doi.org/10.1016/B978-0-12-824360-2.00024-3

Hermann, J. 1997. The Braccia gabbro (Malenco, Alps): Permian intrusion at the crust to mantle interface and Jurassic exhumation during rifting. PhD Thesis, ETH Zurich.

Hiess, J., Condon, D.J., McLean, N., Noble, S.R. 2012. $^{238}U/^{235}U$ Systematics in Terrestrial Uranium-Bearing Minerals. Science, 335, 1610–1614, https://doi.org/10.1126/science.1215507

Hoffmann, U., Breitkreuz, C., Breiter, K., Sergeev, S., Stanek, K., Tichomirowa, M. 2013. Carboniferous–Permian volcanic evolution in Central Europe—U/Pb ages of volcanic rocks in Saxony (Germany) and northern Bohemia (Czech Republic). International Journal of Earth Sciences, 102, 73–99, https://doi.org/10.1007/s00531-012-0791-2

Huff, W.D. 2016. K-bentonites: A review. American Mineralogist, 101, 43–70, https://doi.org/10.2138/am-2016-5339

Isbell, J.L., Henry, L.C., Gulbranson, E.L., Limarino, C.O., Fraiser, M.L., Koch, Z.J., Ciccioli, P.L., Dineen, A.A. 2012. Glacial paradoxes during the late Paleozoic ice age: Evaluating the equilibrium line altitude as a control on glaciation. Gondwana Research, 22, 1–19, https://doi.org/10.1016/j.gr.2011.11.005

Izart, A., Palhol, F., Gleixner, G., Elie, M., Blaise, T., Suarez-Ruiz, I., Sachsenhofer, R.F., Privalov, V.A., Panova, E.A. 2012. Palaeoclimate reconstruction from biomarker geochemistry and stable isotopes of n-alkanes from Carboniferous and Early Permian humic coals and limnic sediments in western and eastern Europe. Organic Geochemistry, 43, 125–149, https://doi.org/10.1016/j.orggeochem.2011.10.004

Jaffey, A.H., Flynn, K.F., Glendenin, L.E., Bentley, W.C., Essling, A.M. 1971. Precision Measurement of Half-Lives and Specific Activities of ^{235}U and ^{238}U. Physical Review C, 4, 1889–1906, https://doi.org/10.1103/PhysRevC.4.1889

Jarvis, I., Jarvis, K.E. 1985. Rare-earth element geochemistry of standard sediments: A study using inductively coupled plasma spectrometry. Chemical Geology, 53, 335–344, https://doi.org/10.1016/0009-2541(85)90078-6

Jirásek, J., Opluštil, S., Sivek, M., Schmitz, M.D., Abels, H.A. 2018. Astronomical forcing of Carboniferous paralic sedimentary cycles in the Upper Silesian Basin, Czech Republic (Serpukhovian, latest Mississippian): New radiometric ages afford an astronomical age model

for European biozonations and substages. Earth Science Reviews, 177, 715–741, https://doi.org/10.1016/j.earscirev.2017.12.005

Kent, D.V., Muttoni, G. 2020. Pangea B and the Late Paleozoic Ice Age. Palaeogeography, Palaeoclimatology, Palaeoecology, 553, 109753, https://doi.org/10.1016/j.palaeo.2020.109753

Knight, J.A., Wagner, R.H. 2014. Proposal for the recognition of a Saberian Substage in the mid-Stephanian (West European chronostratigraphic scheme). Freiberger Forschungshefte C, Paläontologie, Stratigraphie, Fazies, 548, 179–195.

Königer, S., Stollhofen, H. 2001. Environmental and Tectonic Controls on Preservation Potential of Distal Fallout Ashes in Fluvio-Lacustrine Settings: The Carboniferous–Permian Saar–Nahe Basin, South–West Germany. In: White, J.D.L., Riggs, N.R. (eds) Volcaniclastic Sedimentation in Lacustrine Settings. Blackwell Publishing Ltd., Oxford, UK, 263–284, https://doi.org/10.1002/9781444304251.ch13

Krogh, T.E. 1973. A low-contamination method for hydrothermal decomposition of zircon and extraction of U and Pb for isotopic age determinations. Geochimica Cosmochimica Acta, 37, 485–494, https://doi.org/10.1016/0016-7037(73)90213-5

Langiaux, J. 1984. Flores et faunes des formations supérieures du Stéphanien de Blanzy-Montceau (Massif central français) : stratigraphie et paléoécologie. PhD thesis, Université de Bourgogne.

Larson, K. P., Godin, L., Davis, W. J., & Davis, D. W. 2010. Relationships between displacement and distortion in orogens: Linking the Himalayan foreland and hinterland in central Nepal. Geological Society of America Bulletin, 122, 1116–1134, https://doi.org/10.1130/B30073.1

Laurent, O., Couzinié, S., Zeh, A., Vanderhaeghe, O., Moyen, J.-F., Villaros, A., Gardien, V., Chelle-Michou, C. 2017. Protracted, coeval crust and mantle melting during Variscan late-orogenic evolution: U–Pb dating in the eastern French Massif Central. International Journal of Earth Sciences, 106, 421–451, https://doi.org/10.1007/s00531-016-1434-9

Lloret, J., Ronchi, A., López-Gómez, J., Gretter, N., De la Horra, R., Barrenechea, J.F., Arche, A. 2018. Syn-tectonic sedimentary evolution of the continental late Palaeozoic-early Mesozoic Erill Castell-Estac Basin and its significance in the development of the central Pyrenees Basin. Sedimentary Geology, 374, 134–157, https://doi.org/10.1016/j.sedgeo.2018.07.014

Lopez, M., Gand, G., Garric, J., Körner, F., & Schneider, J. (2008). The playa environments of the Lodève Permian basin (Languedoc-France). Journal of Iberian Geology, 34, 29–56.

Lucas, S.G., Shen, S.-Z. 2018. The Permian chronostratigraphic scale: history, status and prospectus.Geological Society, London, Special Publications, 50, 21–50, https://doi.org/10.1144/SP450.3

Luccisano, V., Pradel, A., Amiot, R., Pouillon, J.-M., Kindlimann, R., Steyer, J.S., Cuny, G. 2022. Systematics, ontogeny and palaeobiogeography of the genus Orthacanthus (Diplodoselachidae, Xenacanthiformes) from the lower Permian of France. Papers in Palaeontology, 8, e1470, https://doi.org/10.1002/spp2.1470

Lützner, H., Tichomirowa, M., Käßner, A., Gaupp, R. 2021. Latest Carboniferous to early Permian volcano-stratigraphic evolution in Central Europe: U–Pb CA–ID–TIMS ages of volcanic rocks in the Thuringian Forest Basin (Germany). International Journal of Earth Sciences, 110, 377–398, https://doi.org/10.1007/s00531-020-01957-y

Malavieille, J., Guihot, P., Costa, S., Lardeaux, J.M., Gardien, V. 1990. Collapse of the thickened Variscan crust in the French Massif Central: Mont Pilat extensional shear zone and St. Etienne Late Carboniferous basin. Tectonophysics, 177, 139–149, https://doi.org/10.1016/0040-1951(90)90278-G

Marcoux, E., Le Berre, P., Cocherie, A. 2004. The Meillers Autunian hydrothermal chalcedony: first evidence of a ~295 Ma auriferous epithermal sinter in the French Massif Central. Ore Geology Reviews, 25, 69–87, https://doi.org/10.1016/j.oregeorev.2003.10.001

Marocchi, M., Morelli, C., Mair, V., Klötzli, U., Bargossi, G.M. 2008. Evolution of Large Silicic Magma Systems: New U-Pb Zircon Data on the NW Permian Athesian Volcanic Group (Southern Alps, Italy). The Journal of Geology, 116, 480–498, https://doi.org/10.1086/590135

Marteau, P. 1983. Le bassin permo-carbonifère d'Autun : stratigraphie, sédimentologie et aspects structuraux. PhD thesis, Université de Bourgogne.

Marx, J., Huebscher, H.-D., Hoth, K., Korich, D., Kramer, W. 1995. Vulkanostratigraphie und Geochemie der Eruptivkomplexe. Norddeutsches Rotliegendbecken. Rotliegend-Monographie Teil, 2, 54–83.

Mascle, A. 1990. Géologie pétrolière des bassins permiens français. Comparaison avec les bassins permiens du Nord de l'Europe. Chronique de la recherche minière, 499, 69–86.

Mathis, V., Brulhet, J. 1990. Les gisements uranifères du bassin permien de Bourbon-l'Archambault (nord du Massif central français). Chronique de la Recherche Minière, 499, 19–30.

Mattinson, J.M. 2005. Zircon U–Pb chemical abrasion ("CA-TIMS") method: Combined annealing and multi-step partial dissolution analysis for improved precision and accuracy of zircon ages. Chemical Geology, 220, 47–66, https://doi.org/10.1016/j.chemgeo.2005.03.011

McCann, T. (ed) 2008. The Geology of Central Europe: Volume 1: Precambrian and Palaeozoic. Geological Society of London.

McLean, N.M., Bowring, J.F., Bowring, S.A. 2011. An algorithm for U-Pb isotope dilution data reduction and uncertainty propagation. Geochemistry, Geophysics, Geosystems, 12, https://doi.org/10.1029/2010GC003478

McLean, N.M., Condon, D.J., Schoene, B., Bowring, S.A. 2015. Evaluating uncertainties in the calibration of isotopic reference materials and multi-element isotopic tracers (EARTHTIME Tracer Calibration Part II). Geochimica and Cosmochimica Acta, 164, 481–501, https://doi.org/10.1016/j.gca.2015.02.040

Ménard, G., Molnar, P. 1988. Collapse of a Hercynian Tibetan Plateau into a late Palaeozoic European Basin and Range province. Nature, 334, 235–237, https://doi.org/10.1038/334235a0

Menning, M., Alekseev, A.S., Chuvashov, B.I., Davydov, V.I., Devuyst, F.-X., Forke, H.C., Grunt, T.A., Hance, L., Heckel, P.H., Izokh, N.G., Jin, Y.-G., Jones, P.J., Kotlyar, G.V., Kozur, H.W., Nemyrovska, T.I., Schneider, J.W., Wang, X.-D., Weddige, K., Weyer, D., Work, D.M. 2006. Global time scale and regional stratigraphic reference scales of Central and West Europe, East Europe, Tethys, South China, and North America as used in the Devonian–Carboniferous–Permian Correlation Chart 2003 (DCP 2003). Palaeogeography, Palaeoclimatology, Palaeoecology, 240, 318–372, https://doi.org/10.1016/j.palaeo.2006.03.058

Mercuzot, M., Bourquin, S., Beccaletto, L., Ducassou, C., Rubi, R., Pellenard, P. 2021a. Palaeoenvironmental reconstitutions at the Carboniferous–Permian transition south of the Paris Basin, France: implications on the stratigraphic evolution and basin geometry. International Journal of Earth Sciences, 110, 9–33, https://doi.org/10.1007/s00531-020-01940-7

Mercuzot, M., Thomazo, C., Schnyder, J., Pellenard, P., Baudin, F., Pierson-Wickmann, A.-C., Sans-Jofre, P., Bourquin, S., Beccaletto, L., Santoni, A.-L., Gand, G., Buisson, M., Glé, L., Munier, T., Saloume, A., Boussaid, M., Boucher, T. 2021b. Carbon and Nitrogen Cycle Dynamic in Continental Late-Carboniferous to Early Permian Basins of Eastern Pangea (Northeastern Massif Central, France). Frontiers in Earth Science, 9, 705351, https://doi.org/10.3389/feart.2021.705351

Mercuzot, M., Bourquin, S., Pellenard, P., Beccaletto, L., Schnyder, J., Baudin, F., Ducassou, C., Garel, S., Gand, G. 2022. Reconsidering Carboniferous–Permian continental paleoenvironments in eastern equatorial Pangea: facies and sequence stratigraphy investigations in the Autun Basin (France). International Journal of Earth Sciences, 111, 1663–1696, https://doi.org/10.1007/s00531-022-02200-6

Michel, L.A., Tabor, N.J., Montañez, I.P., Schmitz, M.D., Davydov, V.I. 2015. Chronostratigraphy and Paleoclimatology of the Lodève Basin, France: Evidence for a pan-tropical aridification event across the Carboniferous–Permian boundary. Palaeogeography, Palaeoclimatology, Palaeoecology, 430, 118–131, https://doi.org/10.1016/j.palaeo.2015.03.020

Miller, J.S., Matzel, J.E.P., Miller, C.F., Burgess, S.D., Miller, R.B. 2007. Zircon growth and recycling during the assembly of large, composite arc plutons. Journal of Volcanology and Geothermal Research, Large Silicic Magma Systems, 167, 282–299, https://doi.org/10.1016/j.jvolgeores.2007.04.019

Monjoie, P., Bussy, F., Schaltegger, U., Mulch, A., Lapierre, H., Pfeifer, H.-R. 2007. Contrasting magma types and timing of intrusion in the Permian layered mafic complex of Mont Collon (Western Alps, Valais, Switzerland): evidence from U/Pb zircon and $^{40}Ar/^{39}Ar$ amphibole

dating. Swiss Journal of Geosciences, 100, 125–135, https://doi.org/10.1007/s00015-007-1210-8

Montañez, I.P., Poulsen, C.J. 2013. The Late Paleozoic Ice Age: An Evolving Paradigm. Annual Review of Earth and Planetary Sciences, 41, 629–656, https://doi.org/10.1146/annurev.earth.031208.100118

Mujal, E., Fortuny, J., Marmi, J., Dinarès-Turell, J., Bolet, A., Oms, O. 2018. Aridification across the Carboniferous–Permian transition in central equatorial Pangea: The Catalan Pyrenean succession (NE Iberian Peninsula). Sedimentary Geology, 363, 48–68, https://doi.org/10.1016/j.sedgeo.2017.11.005

Müller, A.B., Strauss, H., Hartkopf-Fröder, C., Littke, R. 2006. Reconstructing the evolution of the latest Pennsylvanian–earliest Permian Lake Odernheim based on stable isotope geochemistry and palynofacies: A case study from the Saar-Nahe Basin, Germany. Palaeogeography, Palaeoclimatology, Palaeoecology, 240, 204–224, https://doi.org/10.1016/j.palaeo.2006.03.049

Neumann, E.-R., Wilson, M., Heeremans, M., Spencer, E.A., Obst, K., Timmerman, M.J., Kirstein, L. 2004. Carboniferous-Permian rifting and magmatism in southern Scandinavia, the North Sea and northern Germany: a review. Geological Society, London, Special Publications, 223, 11–40, https://doi.org/10.1144/GSL.SP.2004.223.01.02

Nosenzo, F., Manzotti, P., Poujol, M., Ballèvre, M., Langlade, J. 2022. A window into an older orogenic cycle: P–T conditions and timing of the pre-Alpine history of the Dora-Maira Massif (Western Alps). Journal of Metamorphic Geology, 40, 789–821, https://doi.org/10.1111/jmg.12646

Opluštil, S., Lojka, R., & Pšenika, J. (2013). Late Variscan continental basins in western Bohemia: tectono-sedimentary, climate and biotic archives. Schriftreihe Dtsch. Ges. Geowiss., 82, 179–201.

Opluštil, S., Schmitz, M., Cleal, C.J., Martínek, K. 2016a. A review of the Middle–Late Pennsylvanian west European regional substages and floral biozones, and their correlation to the Geological Time Scale based on new U–Pb ages. Earth-Science Reviews, 154, 301–335, https://doi.org/10.1016/j.earscirev.2016.01.004

Opluštil, S., Schmitz, M., Kachlík, V., Štamberg, S. 2016b. Re-Assessment of Lithostratigraphy, Biostratigraphy, and Volcanic Activity of the Late Paleozoic Intra-Sudetic, Krkonoše-Piedmont and Mnichovo Hradiště Basins (Czech Republic) Based on New U-Pb CA-ID-TIMS Ages. Bulletin of Geosciences, 91, 399–432, https://doi.org/10.3140/bull.geosci.1603

Opluštil, S., Cleal, C.J., Wang, J., Wan, M. 2022. Carboniferous macrofloral biostratigraphy: an overview. Geological Society, London, Special Publications, 512, 813–863, https://doi.org/10.1144/SP512-2020-97

Palmer, B.A., Shawkey, E.P. 1997. Lacustrine sedimentation processes and patterns during effusive and explosive volcanism, Challis volcanic field, Idaho. Journal of Sedimentary Research, 67, 154–167, https://doi.org/10.1306/D426851D-2B26-11D7-8648000102C1865D

Paquette, J.-L. 1980. Le Bassin autunien de l'Aumance (Allier) : sédimentologie (charbon, cinérites...), tectonique syndiagénétique. PhD thesis, Université de Bourgogne.

Paquette, J.-L., Feys, R. 1989. Le bassin de l'Aumance. In: Châteauneuf, J.J. and Farjanel, G. (eds) Synthèse Géologique Des Bassins Permiens Français. Mémoires du BRGM, Orléans, France.

Parnell, A.C., Haslett, J., Allen, J.R.M., Buck, C.E., Huntley, B. 2008. A flexible approach to assessing synchroneity of past events using Bayesian reconstructions of sedimentation history. Quaternary Science Reviews, 27, 1872–1885, https://doi.org/10.1016/j.quascirev.2008.07.009

Pellenard, P., Deconinck, J.-F., Huff, W.D., Thierry, J., Marchand, D., Fortwengler, D., Trouiller, A. 2003. Characterization and correlation of Upper Jurassic (Oxfordian) bentonite deposits in the Paris Basin and the Subalpine Basin, France. Sedimentology, 50, 1035–1060, https://doi.org/10.1046/j.1365-3091.2003.00592.x

Pellenard, P., Nomade, S., Martire, L., De Oliveira Ramalho, F., Monna, F., Guillou, H. 2013. The first ^{40}Ar–^{39}Ar date from Oxfordian ammonite-calibrated volcanic layers (bentonites) as a tie-point for the Late Jurassic. Geological Magazine, 150, 1136–1142, https://doi.org/10.1017/S0016756813000605

Pellenard, P., Gand, G., Schmitz, M., Galtier, J., Broutin, J., Stéyer, J.-S. 2017. High-precision U-Pb zircon ages for explosive volcanism calibrating the NW European continental Autunian stratotype. Gondwana Research, 51, 118–136, https://doi.org/10.1016/j.gr.2017.07.014

Pereira, M.F., Castro, A., Chichorro, M., Fernández, C., Díaz-Alvarado, J., Martí, J., Rodríguez, C. 2014. Chronological link between deep-seated processes in magma chambers and eruptions: Permo-Carboniferous magmatism in the core of Pangaea (Southern Pyrenees). Gondwana Research, 25, 290–308, https://doi.org/10.1016/j.gr.2013.03.009

Petschick, R. (ed) 2001. MacDiff–The user-friendly X-ray powder diffractometry analysis tool for Macintosh computers.

Pfefferkorn, H.W. 2023. Pennsylvanian-age plant macrofossil biostratigraphy in tropical Pangaea: uniformitarianism, catastrophes and the 'Cantabrian' problem. Geological Society, London, Special Publications, 535, SP535-2022–282, https://doi.org/10.1144/SP535-2022-282

Pfeifer, L.S., Soreghan, G.S., Pochat, S., Van Den Driessche, J. 2020. Loess in eastern equatorial Pangea archives a dusty atmosphere and possible upland glaciation. GSA Bulletin, 133, 379–392, https://doi.org/10.1130/B35590.1

Pfeifer, L.S., Birkett, B.A., Van Den Driessche, J., Pochat, S., Soreghan, G.S. 2021. Ice-crystal traces imply ephemeral freezing in early Permian equatorial Pangea. Geology, 49, 1397–1401.

Pochat, S., Van Den Driessche, J. 2011. Filling sequence in Late Paleozoic continental basins: A chimera of climate change? A new light shed given by the Graissessac–Lodève basin (SE France). Palaeogeography, Palaeoclimatology, Palaeoecology, 302, 170–186, https://doi.org/10.1016/j.palaeo.2011.01.006

Pochat, S., Van Den Driessche, J. 2016. Comment on "Chronostratigraphy and Paleoclimatology of the Lodève Basin, France: Evidence for a pan-tropical aridification event across the Carboniferous–Permian boundary" by Michel, L. A., Tabor, N. J., Montañez, I. P., Schmitz, M. D., & Davydov, V. I. (2015). Palaeogeography, Palaeoclimatology, Palaeoecology, 430, 118–131. Palaeogeography, Palaeoclimatology, Palaeoecology, 441, 997–999, https://doi.org/10.1016/j.palaeo.2015.10.024

Poplin, C. 1999. Un paléoniscoïde (Pisces, Actinopterygii) de Buxières-les-Mines, témoin des affinités fauniques entre Massif central et Bohême au passage Carbonifère-Permien. Geodiversitas, 21, 147–155.

Poujol, M., Mercuzot, M., Lopez, M., Bourquin, S., Bruguier, O., Hallot, E., Beccaletto, L. 2023. Insights on the Permian volcanic ash beds from the Saint-Affrique Basin (Massif Central, France): An integrated geochemical and geochronological study. Comptes Rendus Géoscience, 355, 1–25.

Primey, D., Farjanel, G. 1989. Etude paléobotanique et palynologique des gisements stéphano-autuniens de Lucenay-lès-Aix et Devay (Bassin de Decize, Nièvre). Document du BRGM, 178.

Ramezani, J., Schmitz, M.D., Davydov, V.I., Bowring, S.A., Snyder, W.S., Northrup, C.J. 2007. High-precision U–Pb zircon age constraints on the Carboniferous–Permian boundary in the southern Urals stratotype. Earth and Planetary Science Letters, 256, 244–257, https://doi.org/10.1016/j.epsl.2007.01.032

Ramezani, J., Hoke, G.D., Fastovsky, D.E., Bowring, S.A., Therrien, F., Dworkin, S.I., Atchley, S.C., Nordt, L.C. 2011. High-precision U-Pb zircon geochronology of the Late Triassic Chinle Formation, Petrified Forest National Park (Arizona, USA): Temporal constraints on the early evolution of dinosaurs. GSA Bulletin, 123, 2142–2159, https://doi.org/10.1130/B30433.1

Ramezani, J., Beveridge, T.L., Rogers, R.R., Eberth, D.A., Roberts, E.M. 2022. Calibrating the zenith of dinosaur diversity in the Campanian of the Western Interior Basin by CA-ID-TIMS U–Pb geochronology. Scientific Reports, 12, 16026, https://doi.org/10.1038/s41598-022-19896-w

Rodríguez-Méndez, L., Cuevas, J., Esteban, J.J., Tubía, J.M., Sergeev, S., Larionov, A. 2014. Age of the magmatism related to the inverted Stephanian–Permian basin of the Sallent area (Pyrenees). Geological Society, London, Special Publications, 394, 101–111, https://doi.org/10.1144/SP394.2

Ronchi, A., Sarria, E., & Broutin, J. (2008). The "Autuniano Sardo": basic features for a correlation through the Western Mediterranean and Paleoeurope. Bollettino della Società Geologica Italiana, 127, 655–681.

Roscher, M., Schneider, J.W. 2005. An annotated correlation chart for continental Late Pennsylvanian and Permian basins and the marine scale. The Nonmarine Permian. New Mexico Museum of Natural History and Science Bulletin, 30, 282–291.

Roscher, M., Schneider, J.W. 2006. Permo-Carboniferous climate: Early Pennsylvanian to Late Permian climate development of central Europe in a regional and global context. Geological Society, London, Special Publications, 265, 95–136, https://doi.org/10.1144/GSL.SP.2006.265.01.05

Schaltegger, U., Brack, P. 2007. Crustal-scale magmatic systems during intracontinental strike-slip tectonics: U, Pb and Hf isotopic constraints from Permian magmatic rocks of the Southern Alps. International Journal of Earth Sciences, 96, 1131–1151, https://doi.org/10.1007/s00531-006-0165-8

Schmitz, M.D., Davydov, V.I. 2012. Quantitative radiometric and biostratigraphic calibration of the Pennsylvanian–Early Permian (Cisuralian) time scale and pan-Euramerican chronostratigraphic correlation. GSA Bulletin, 124, 549–577, https://doi.org/10.1130/B30385.1

Schneider, J.W., Zajíc, J. 1994. Xenacanthiden (Pisces, Chondrichthyes) des mitteleuropäischen Oberkarbon und Perm–Revision der Originale zu Goldfuss 1847, Beyrich 1848, Kner 1867 und Fritsch 1879–1890. Freiberger Forschungshefte C, 452, 101–151.

Schneider, J.W., Hampe, O., Soler-Gijón, R. 2000. The Late Carboniferous and Permian: aquatic vertebrate zonation in southern Spain and German basins. Courier-Forschungsinstitut Senckenberg, 2000, 543–562.

Schneider, J.W., Körner, F., Roscher, M., Kroner, U. 2006. Permian climate development in the northern peri-Tethys area — The Lodève basin, French Massif Central, compared in a European and global context. Palaeogeography, Palaeoclimatology, Palaeoecology, 240, 161–183, https://doi.org/10.1016/j.palaeo.2006.03.057

Schneider, J.W., Werneburg, R. 2006. Insect biostratigraphy of the Euramerican continental Late Pennsylvanian and Early Permian. Geological Society, London, Special Publications, 265, 325–336, https://doi.org/10.1144/GSL.SP.2006.265.01.15

Schneider, J.W., Scholze, F. 2018. Late Pennsylvanian–Early Triassic conchostracan biostratigraphy: a preliminary approach. Geological Society, London, Special Publications, 450, 365–386, https://doi.org/10.1144/SP450.6

Schneider, J.W., Lucas, S.G., Scholze, F., Voigt, S., Marchetti, L., Klein, H., Opluštil, S., Werneburg, R., Golubev, V.K., Barrick, J.E., Nemyrovska, T., Ronchi, A., Day, M.O., Silantiev, V.V., Rößler, R., Saber, H., Linnemann, U., Zharinova, V., Shen, S.-Z. 2020. Late Paleozoic–early Mesozoic continental biostratigraphy — Links to the Standard Global Chronostratigraphic Scale. Palaeoworld, 29, 186–238, https://doi.org/10.1016/j.palwor.2019.09.001

Shen, S., Zhang, H., Zhang, Y., Yuan, D., Chen, B., He, W., Mu, L., Lin, W., Wang, W., Chen, J., Wu, Q., Cao, C., Wang, Y., Wang, X. 2019. Permian integrative stratigraphy and timescale of China. Science China Earth Sciences, 62, 154–188, https://doi.org/10.1007/s11430-017-9228-4

Soreghan, G.S., Soreghan, M.J., Heavens, N.G. 2019. Explosive volcanism as a key driver of the late Paleozoic ice age. Geology 47, 600–604, https://doi.org/10.1130/G46349.1

Spears, D.A. 1970. A Kaolinite Mudstone (Tonstein) in the British Coal Measures. Journal of Sedimentary Research, 40.

Spears, D.A. 2012. The origin of tonsteins, an overview, and links with seatearths, fireclays and fragmental clay rocks. International Journal of Coal Geology, 94, 22–31, https://doi.org/10.1016/j.coal.2011.09.008

Spillmann, P., Büchi, H.J. 1993. The Pre-Alpine Basement of the Lower Austro-Alpine Nappes in the Bernina Massif (Grisons, Switzerland; Valtellina, Italy). In: von Raumer, J.F., Neubauer, F. (eds) Pre-Mesozoic Geology in the Alps. Springer, Berlin, Heidelberg, 457–467, https://doi.org/10.1007/978-3-642-84640-3_27

Srodón, J. (ed) 1976. Mixed-layer smectite/illites in the Bentonites and Tonsteins of the Upper Silesian coal basin.

Štamberg, S., Steyer, J.-S. 2021. New actinopterygians from the Permian of the Brive Basin, and the ichthyofaunas of the French Massif Central. Fossil Imprint, 77, 145–165.

Stampfli, G.M., Kozur, H.W. 2006. Europe from the Variscan to the Alpine cycles. Journal of the Geological Society of London, 32, 57–82, https://doi.org/10.1144/GSL.MEM.2006.032.01.04

Stollhofen, H. 1998. Facies architecture variations and seismogenic structures in the Carboniferous–Permian Saar–Nahe Basin (SW Germany): evidence for extension-related transfer fault activity. Sedimentary Geology, 119, 47–83, https://doi.org/10.1016/S0037-0738(98)00040-2

Timmerman, M.J. 2004. Timing, geodynamic setting and character of Permo-Carboniferous magmatism in the foreland of the Variscan Orogen, NW Europe. Geological Society, London, Special Publications, 223, 41–74, https://doi.org/10.1144/GSL.SP.2004.223.01.03

Timmerman, M.J. Heeremans, M., Kirstein, L.A., Larsen, B.T., Spencer-Dunworth, E.-A., Sundvoll, B., 2009. Linking changes in tectonic style with magmatism in northern Europe during the late Carboniferous to latest Permian. Tectonophysics, 473, 375–390, https://doi.org/10.1016/j.tecto.2009.03.011

Tribuzio, R., Thirlwall, M.F., Messiga, B. 1999. Petrology, mineral and isotope geochemistry of the Sondalo gabbroic complex (Central Alps, Northern Italy): implications for the origin of post-Variscan magmatism. Contributions to Mineralogy and Petrology, 136, 48–62, https://doi.org/10.1007/s004100050523

Tribuzio, R., Renna, M.R., Braga, R., Dallai, L. 2009. Petrogenesis of Early Permian olivine-bearing cumulates and associated basalt dykes from Bocca di Tenda (Northern Corsica): Implications for post-collisional Variscan evolution. Chemical Geology, 259, 190–203, https://doi.org/10.1016/j.chemgeo.2008.10.045

Trümper, S., Götze, J., Rößler, R. 2020. Siliceous Petrifactions in the Permian of the Parnaíba Basin, Central-North Brazil: Sedimentary Environment and Fossilization Pathways. In: Iannuzzi, R., Rößler, R., Kunzmann, L. (eds) Brazilian Paleofloras: From Paleozoic to Holocene. Springer International Publishing, Cham, 1–45, https://doi.org/10.1007/978-3-319-90913-4_10-1

Van Den Driessche, J., Brun, J.-P. 1992. Tectonic evolution of the Montagne Noire (French Massif Central): a model of extensional gneiss dome. Geodinamica Acta, 5, 85–97, https://doi.org/10.1080/09853111.1992.11105221

Vanderhaeghe, O., Laurent, O., Gardien, V., Moyen, J. F., Gébelin, A., Chelle-Michou, C., Couzinié, S., Villaros, A., Bellanger, M. 2020. Flow of partially molten crust controlling construction, growth and collapse of the Variscan orogenic belt: the geologic record of the French Massif Central. Bulletin de la Société géologique de France, 191, 1–25, https://doi.org/10.1051/bsgf/2020013

Vermeesch, P. 2018. IsoplotR: A free and open toolbox for geochronology. Geoscience Frontiers, 9, 1479–1493, https://doi.org/10.1016/j.gsf.2018.04.001

Vielzeuf, D., Pin, C. 1989. Geodynamic implications of granulitic rocks in the Hercynian belt. Geological Society, London, Special Publications, 43, 343–348, https://doi.org/10.1144/GSL.SP.1989.043.01.29

Voigt, S., Schindler, T., Tichomirowa, M., Käßner, A., Schneider, J.W., Linnemann, U. 2022. First high-precision U–Pb age from the Pennsylvanian-Permian of the continental Saar–Nahe Basin, SW Germany. International Journal of Earth Sciences, 111, 2129–2147, https://doi.org/10.1007/s00531-022-02222-0

Werneburg, R., Ronchi, A., Schneider, J.W. 2007. The Early Permian Branchiosaurids (Amphibia) of Sardinia (Italy): Systematic Palaeontology, Palaeoecology, Biostratigraphy and Palaeobiogeographic Problems. Palaeogeography, Palaeoclimatology, Palaeoecology, 252, 383–404, https://doi.org/10.1016/j.palaeo.2007.03.048

Wilson, M., Neumann, E.-R., Davies, G.R., Timmerman, M.J., Heeremans, M., Larsen, B.T. 2004. Permo-Carboniferous magmatism and rifting in Europe: introduction. Geological Society, London, Special Publications, 223, 1–10, https://doi.org/10.1144/GSL.SP.2004.223.01.01

Winchester, J.A., Floyd, P.A. 1977. Geochemical discrimination of different magma series and their differentiation products using immobile elements. Chemical Geology, 20, 325–343, https://doi.org/10.1016/0009-2541(77)90057-2

Wray, D.S. 1999. Identification and long-range correlation of bentonites in Turonian–Coniacian (Upper Cretaceous) chalks of northwest Europe. Geological Magazine, 136, 361–371, https://doi.org/10.1017/S0016756899002836

Wu, Q., Ramezani, J., Zhang, H., Wang, J., Zeng, F., Zhang, Y., Liu, F., Chen, J., Cai, Y., Hou, Z., Liu, C., Yang, W., Henderson, C.M., Shen, S. 2021. High-precision U-Pb age constraints on the

Permian floral turnovers, paleoclimate change, and tectonics of the North China block. Geology, 49, 677–681, https://doi.org/10.1130/G48051.1

Zheng, J.S., Mermet, J.-F., Toutin-Morin, N., Hanes, J., Gondolo, A., Morin, R., Féraud, G. 1992. Datation ^{40}Ar–^{39}Ar du magmatisme et de filons minéralisés permiens en Provence orientale (France). Geodinamica Acta, 5, 203–215, https://doi.org/10.1080/09853111.1992.11105228

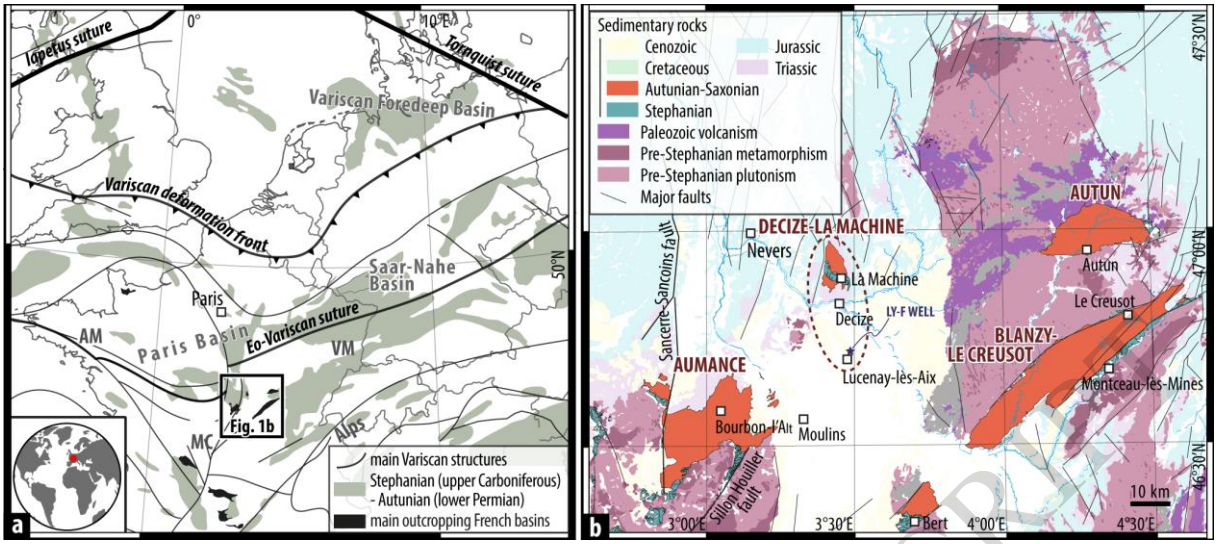

Figure 1

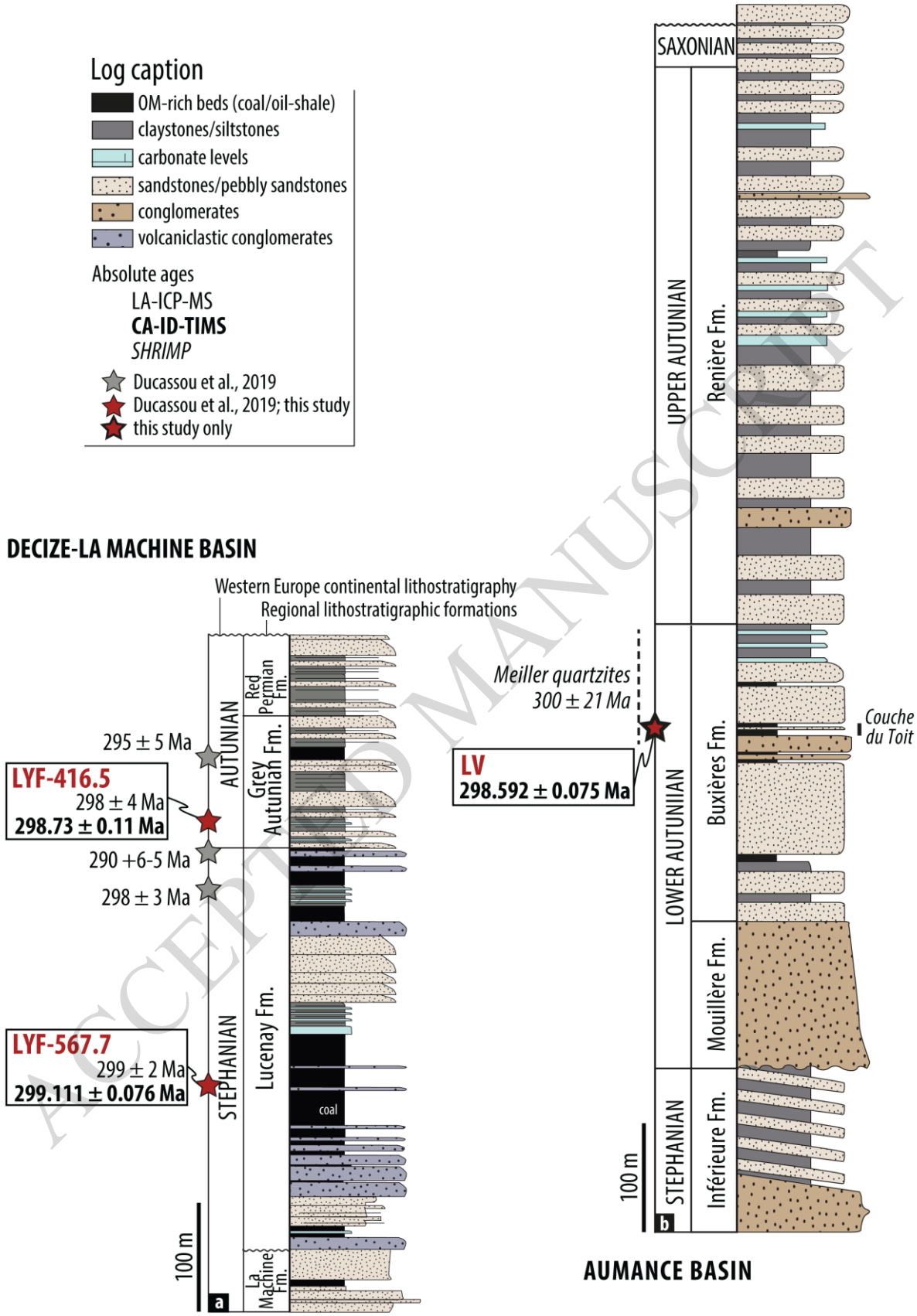

Figure 2

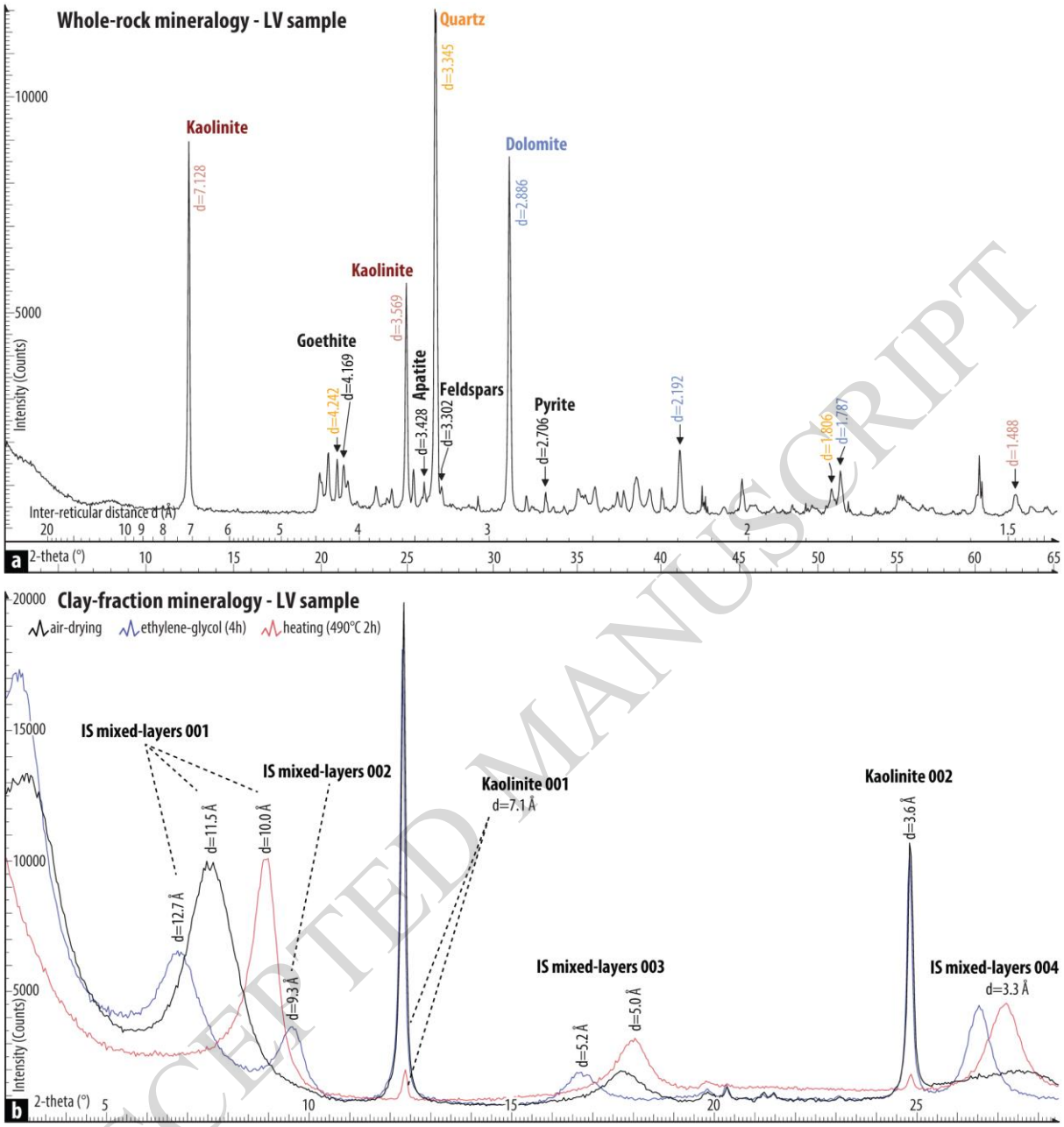

Figure 3

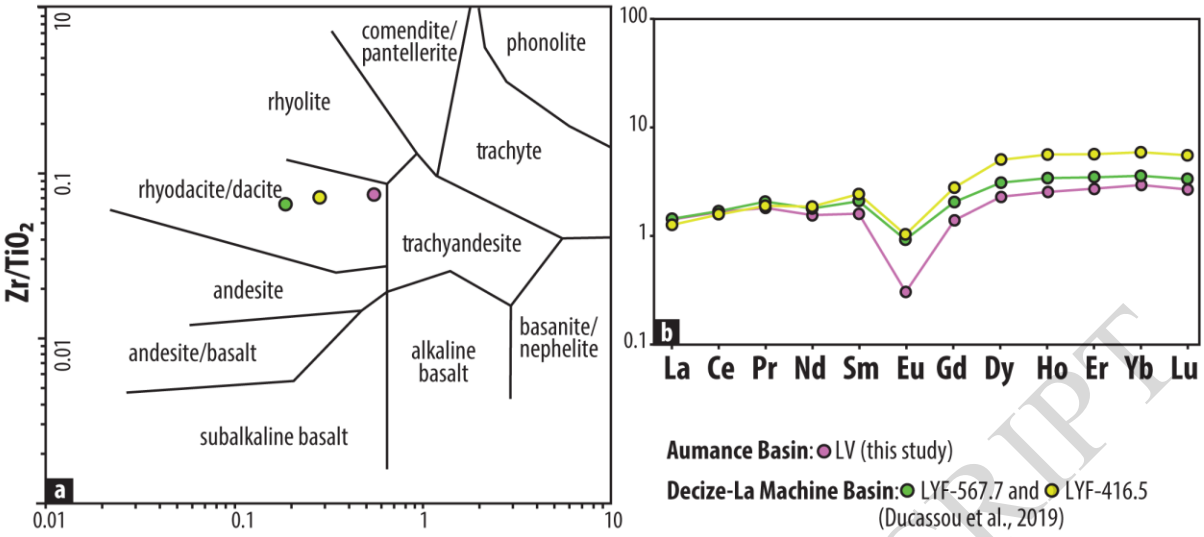

Figure 4

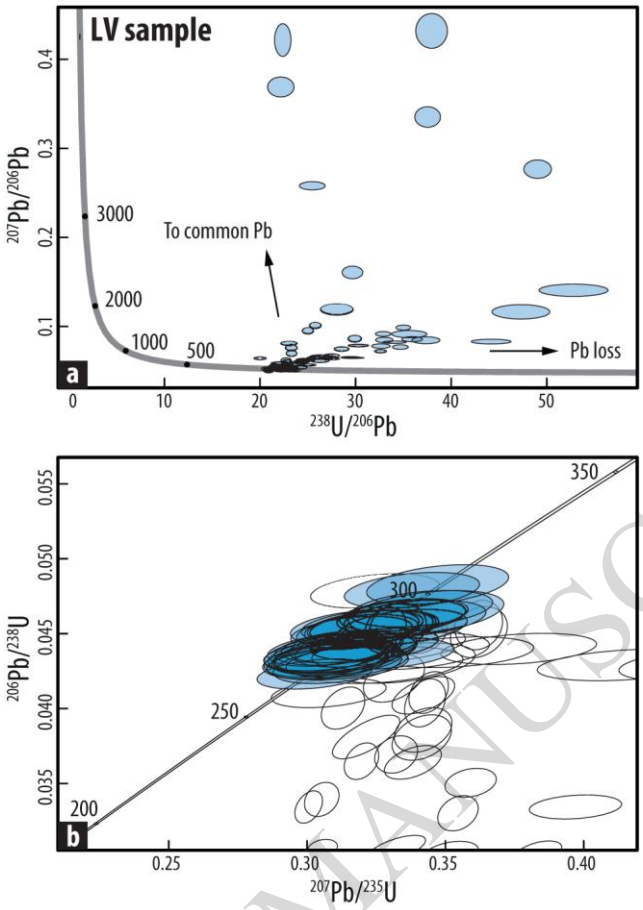

Figure 5

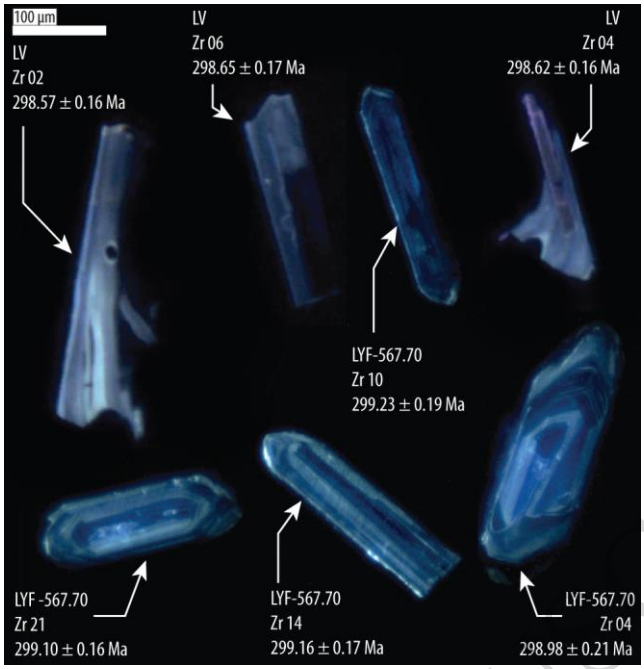

Figure 6

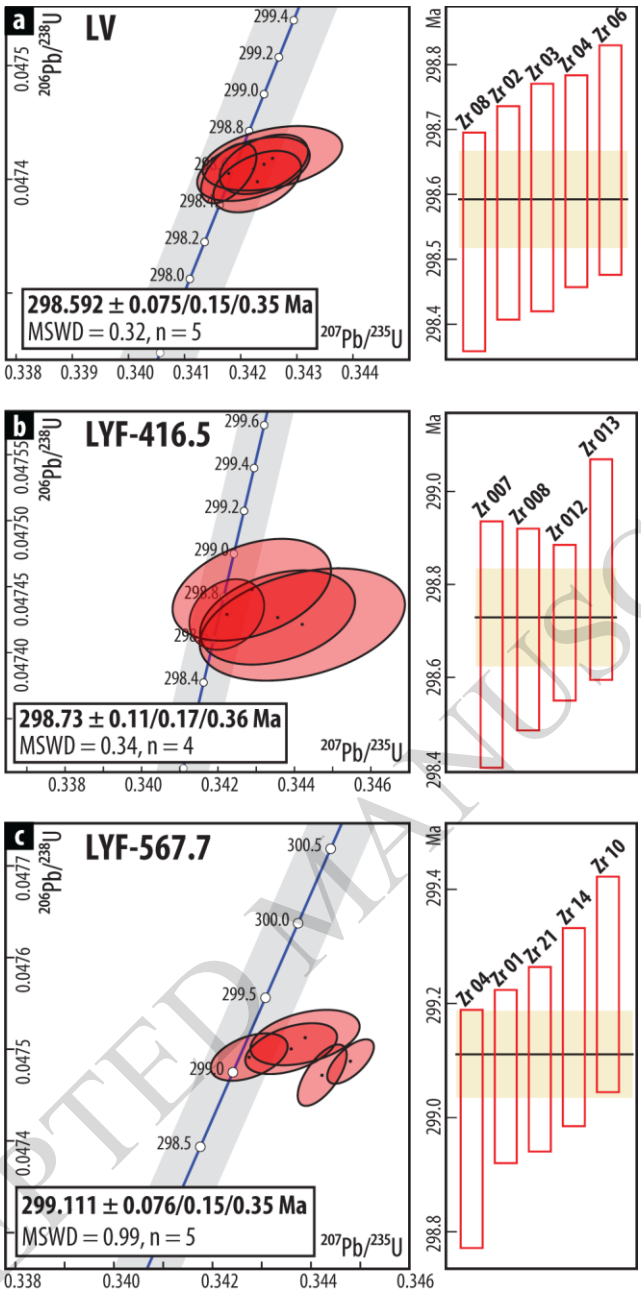

Figure 7

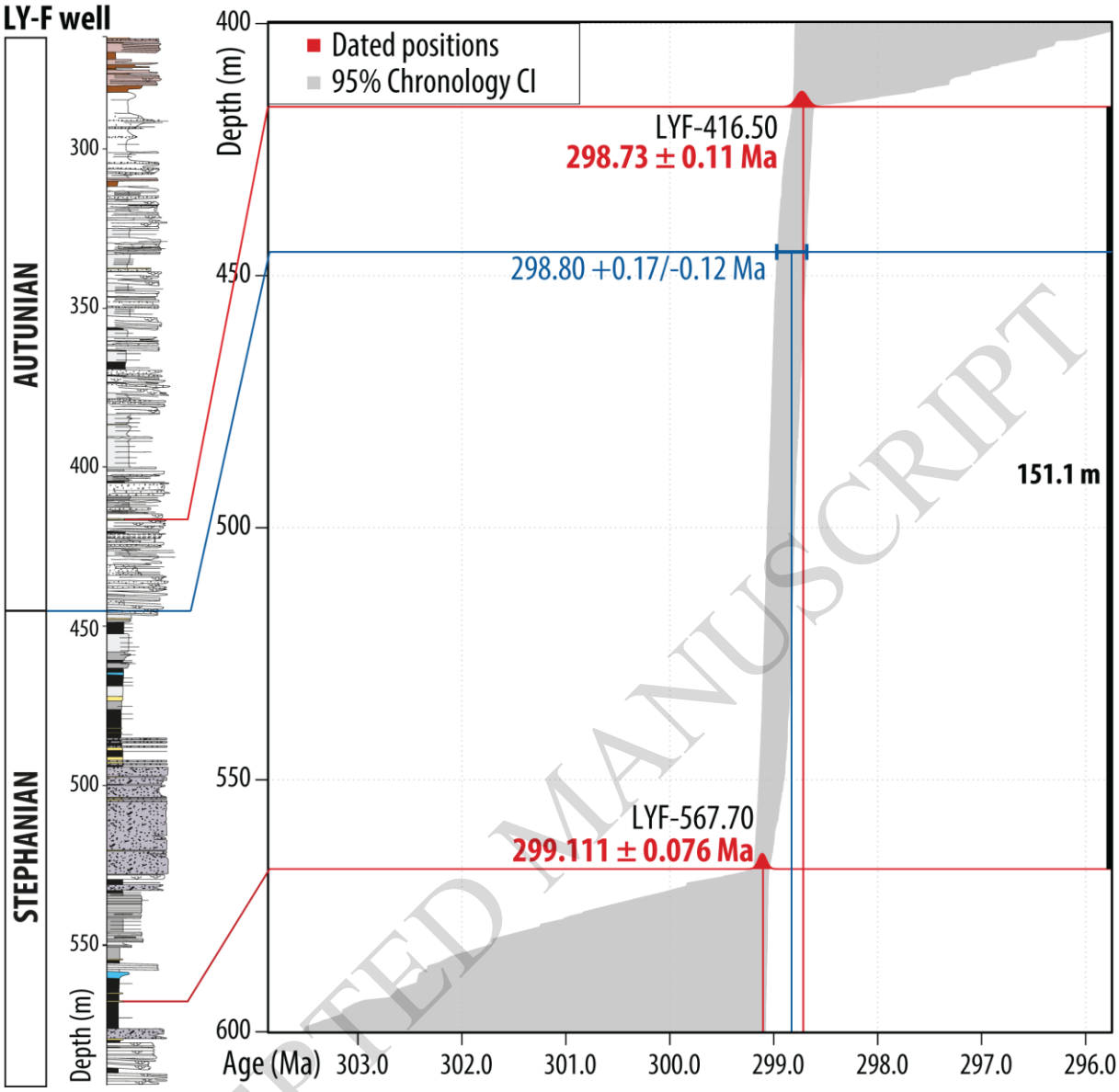

Figure 8

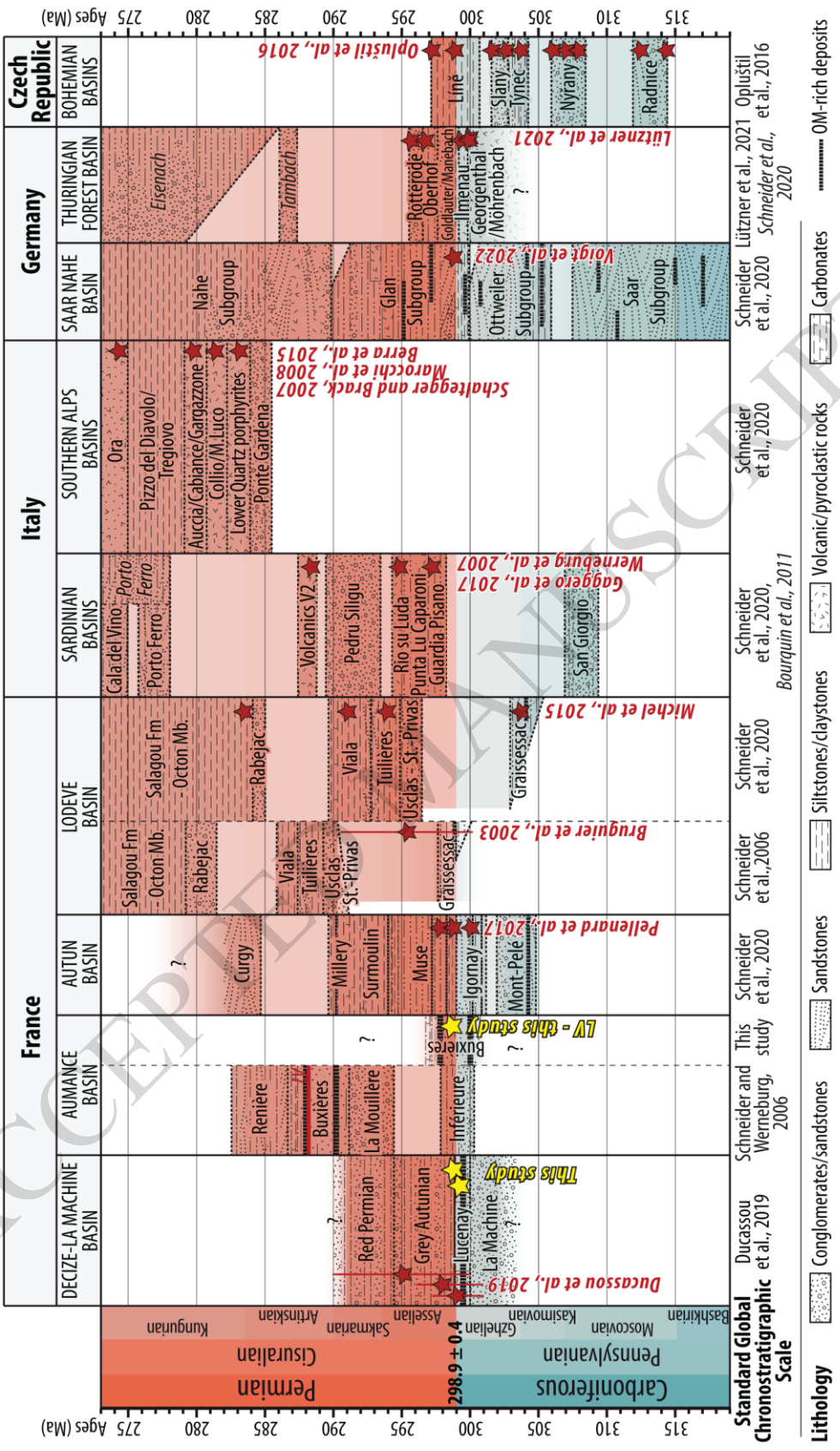

Figure 9

Table 1. *Mineralogical compositions of the clay fraction and the bulk-rock for the LV (Aumance Basin), LYF-416.5 and LYF-567.7 (Decize–La Machine Basin) tonsteins*

		Clay fraction (⌀ < 2 μm, %)				Bulk rock (%)							
Sample	**Basin**	**IS R1**	**I**	**K**	**Qz**	**Clays**	**Qz**	**Carb**	**A**	**Fds**	**Go**	**P**	**G**
LV	Aumance	52†	0	48	0	28	37	28	1	1	3	2	0
LYF-416.5*	Decize–La Machine	12	0	88	0	56	12	2	1	>1	16	>1	13
LYF-567.7*	Decize–La Machine	17	0	75	8	54	37	>1	>1	1	6	1	0

Note: Details of location and stratigraphy are given in Figures 1 and 2, respectively.
Results are rounded to the nearest percent, excepted for values lower than 1%.
*Results from Ducassou et al. (2019); †rectorite
CV—Chlorite-vermiculite mixed-layers; IS R1—Illite-smectite mixed-layers; I—Illite; K—Kaolinite; Qz—Quartz; Carb—Carbonates: dolomite and siderite; A—Apatite; Fds—K-feldspars and plagioclases; Go—Goethite; P—Pyrite; G—Gypsum

Table 2. *Summary of calculated U-Pb dates and their uncertainties*

		LA–ICP–MS					CA–ID–TIMS					
Sample	**Basin**	**Concordia age (Ma)**	**error (2σ)**	**MSWD‡**	**n§**	**No.**	**$^{206}Pb/^{238}U$ Age (Ma)**	**error (2σ)†**			**MSWD‡**	**n§**	**No.**
								X	*Y*	*Z*			
LV	Aumance	**NA**	**NA**	NA	95	95	**298.592**	0.075	0.15	0.35	0.32	5	5
LYF-416.5	Decize–La Machine	***298.0**	**4**	1.16	10	51	**298.73**	0.11	0.17	0.36	0.34	4	5
LYF-567.7	Decize–La Machine	***299.0**	**2**	0.35	17	40	**299.111**	0.076	0.15	0.35	0.99	5	5

Note: Details of location and stratigraphy are given in Figures 1 and 2, respectively.

*Ages from Ducassou et al. (2019).

†*X*—internal (analytical) uncertainty in the absence of all external or systematic errors; *Y*—incorporates the U-Pb tracer calibration error; *Z*—includes X and Y, as well as the uranium decay constant errors.

‡MSWD—mean square of weighted deviates.

n§—number of analyses included in the calculated weighted mean date out of the total number of analyses (No.).